Orbital forcing of tropical climate dynamics in the Early Cambrian

Tan Zhang [a,b], Yifan Li [a,b,*], Tailiang Fan [a], Anne-Christine Da Silva [c], Mingzhi Kuang [d], Wangwei Liu [e], Chao Ma [f], Qi Gao [g], Juye Shi [a], Zhiqian Gao [a], Mingsong Li [h,**]

[a] School of Energy Resources, China University of Geosciences (Beijing), Beijing 100083, China
[b] Key Laboratory of Marine Reservoir Evolution and Hydrocarbon Enrichment Mechanism, Ministry of Education, China University of Geosciences (Beijing), Beijing 100083, China
[c] Sedimentary Petrology Laboratory, Liège University, Sart Tilman B20, Allée du Six Août 12, 4000 Liège, Belgium
[d] College of Energy, Chengdu University of Technology, Chengdu 610059, China
[e] Wuxi Research Institute of Petroleum Geology, Research Institute of Petroleum Exploration and Production, SINOPEC, Wuxi 214151, China
[f] Institute of Sedimentary Geology, State Key Laboratory of Oil and Gas Reservoir Geology and Exploitation, Chengdu University of Technology, Chengdu 610059, China
[g] No.4 Oil Production Plant, Changqing Oilfield Company, Yulin, Shaanxi 718500, China
[h] Key Laboratory of Orogenic Belts and Crustal Evolution, MOE, School of Earth and Space Sciences, Peking University, Beijing 100871, China

ARTICLE INFO

ABSTRACT

According to modern atmospheric circulation models, the Intertropical Convergence Zone (ITCZ), as the Earth's meteorological equator, plays an essential role in the low-latitude hydrologic cycles. The limited availability of high-resolution tropical climate archives, especially from the Early Paleozoic Era, severely limits our understanding of ITCZ migration dynamics in deep time. Here we present high-resolution climate-proxy records (i.e., magnetic susceptibility (MS) and Zirconium/Aluminum (Zr/Al)) from tropical marine sediments of the ~526-million-year-old Qiongzhusi Formation in South China to investigate the link between orbitally forced insolation changes, ITCZ migration dynamics, and low-latitude climate processes. These orbital-scale variations in MS and Zr/Al series are interpreted as alternations between wet and dry cycles, controlled by monsoon intensity under the orbitally forced ITCZ-related paleo-Hadley Cell dynamics. Our results show that combined precession and obliquity orbital cycles had an impact on the Early Cambrian ITCZ migration. Specifically, the precession and obliquity forcing shift the mean position of the ITCZ latitudinally by changing the interhemispheric pressure contrasts, thus affecting the low latitude hydroclimate cycle. We report semi-precession cycles of 8.3–7.9 kyr, which were probably associated with the twice-annual passage of the ITCZ across the intertropical zone, consistent with the paleogeographical location of South China near the equator during the Early Cambrian. Observed ~1.1 – ~1.5 Myr eccentricity amplitude modulation (AM) cycles and ~ 1.0 – ~1.2 Myr obliquity AM cycles may provide geological evidence for the chaotic motion between Earth and Mars in the Early Cambrian.

1. Introduction

The intertropical convergence zone (ITCZ), known as the maximum region in annual average precipitation near the equator, can significantly influence the low latitude hydrological cycle (Broccoli et al., 2006; Schneider et al., 2014; Chiang and Friedman, 2012). Hadley Cells are one of the three critical cells that contribute to modern global atmospheric circulation. They are formed mainly by the ascending flow with moisture-laden air from ITCZ and descending subtropical flow.

These cells lead to dry air at around 25–30° latitude north and south, and they bring abundant rainfall to the region beneath the ascending flow and drought to the region beneath the descending flow (Hofmann and Wagner, 2011; Liu et al., 2015; Wagner et al., 2013; Wang, 2021). Hadley Cell circulation plays a crucial role in climate variations in low latitudes by affecting the monsoonal systems, trade winds, and other oceanic processes (e.g., Hofmann and Wagner, 2011; Mamalakis et al., 2021; Schneider et al., 2014). The geographic distribution of monsoonal precipitation and trade wind intensity shifts regularly with the

migration of the position of the ITCZ in response to seasonal and longer-term variations in solar insolation (e.g., Broccoli et al., 2006; Chiang, 2009; Schneider et al., 2014; Sloan and Huber, 2001). These changes in Hadley Cell dynamics ultimately translate into climate patterns and oceanic circulation alterations at low latitudes (Broccoli et al., 2006; Chiang, 2009; Schneider et al., 2014; Sloan and Huber, 2001). A small migration of the ITCZ position can lead to dramatic changes in rainfall patterns and even to extreme weather events such as floods, droughts and tropical cyclones (Cai et al., 2012). For example, persistent droughts resulting from changes in the position of the ITCZ are thought to have been responsible for the collapse of the Mayan civilization and several Chinese Dynasties (Haug et al., 2001; Yancheva et al., 2007). Generally, the ITCZ position migrates towards the warming hemisphere (e.g., Broccoli et al., 2006; Schneider et al., 2014), as evidenced by a southward migration of boreal-summer ITCZ due to Northern Hemisphere summers cooling from the Holocene thermal maximum at ca. 8 kyr ago until the onset of the Little Ice Age at ca. 0.5 kyr ago (e.g., Haug et al., 2001; Koutavas et al., 2006; Peterson et al., 2000).

Orbitally paced quasi-periodic changes in insolation on Earth's surface, known as Milankovitch cycles, exert significant control on Earth's climate via its influence on the total amount and spatial distribution of the solar irradiance and migration of the atmospheric circulation cells (Berger et al., 1992; Hinnov, 2013; Milankovitch, 1941). Through the Mesozoic and Cenozoic and even in Precambrian times, lines of evidence from past paleoclimate archives suggest that orbitally-forced solar insolation changes would lead to a northward/southward migration of the ITCZ, thus affecting low-latitude climate processes significantly (e. g., Armstrong et al., 2016; Chu et al., 2020; Clement et al., 2004; De Vleeschouwer et al., 2012; Hofmann and Wagner, 2011; Liu et al., 2015; Schneider et al., 2014; Sloan and Huber, 2001; Wang et al., 2004, 2008; Winguth and Winguth, 2013; Zhang et al., 2019, Zhang et al., 2015). Ultimately, these climate changes at low latitudes are recorded into the sediments mainly through regional or local hydrological cycle variations and weathering intensity changes (e.g., Ao et al., 2020; Beckmann et al., 2005; Huang et al., 2020; Liu et al., 2015; Wang et al., 2021). However, high-quality paleoclimate records from equatorial regions in the Early Paleozoic are rare, hindering our understanding of the ITCZ migration dynamics and climate responses in the tropical latitude regions.

According to theoretical models, the motion of the Solar System is chaotic, which results in high uncertainty of numerical solutions beyond 50 million years ago (Laskar, 1990; Laskar, 1989; Laskar et al., 2011b). The Earth's chaotic motion is mainly affected by the Earth-Mars secular resonance and changes in the dynamic ellipticity and tidal dissipation of the Earth-Moon system (Berger et al., 1992; Laskar, 1990; Laskar et al., 2004). The gravitational interaction between Earth and Mars produces Myr-scale long-period modulations in Earth's orbital parameters, currently manifested by a ~2.4 Myr amplitude modulation (AM) of the eccentricity cycles and ~1.2 Myr AM cycle of obliquity (Laskar et al., 2004). These Myr-scale cycles are primarily governed by the g_4-g_3 (i.e., ~2.4 Myr) and s_4-s_3 (~1.2 Myr) of the fundamental frequencies of the Solar System (Laskar et al., 2011a; Laskar et al., 2004). The present libration state of $(g_4$-$g_3)$-$2(s_4$-$s_3)$ =0 (i.e., ~2.4 Myr eccentricity: ~1.2 Myr obliquity) associated with Earth-Mars secular resonance could change throughout time and evolve to libration in a new resonance $(g_4$-$g_3)$-$2(s_4$-$s_3)$ =0 (i.e., ~1.2 Myr eccentricity: ~1.2 Myr obliquity) where g_3 and g_4 terms, as well as s_3 and s_4 terms, are related to the precession of the perihelion and the node of Earth and Mars, respectively. However, the chaotic behavior of the Solar system remains poorly constrained in Paleozoic Era.

Here, high-resolution multi-proxy paleoclimate records from tropical marine sediments of the Early Cambrian Qiongzhusi Formation in the Dongxihe section of South China offer a rare glimpse into the past low-latitude climate processes related to the ITCZ position and its relationship with external climate forcing (i.e., orbital timescale insolation variations). Moreover, stratigraphic records from the Qiongzhusi Formation provide an opportunity to constrain the chaotic behavior of the

Solar system. In this respect, the four main objectives of the present study are: (1) to provide high-resolution astrochronology for the Qiongzhusi Formation, (2) to investigate the underlying link between orbitally induced insolation changes, the ITCZ migration dynamics, and low-latitude climate response, (3) to identify sub-Milankovitch cycles in deep time and the modulation of millennial-scale tropic climate change, (4) to recover the chaotic behavior of the Solar System in the Early Cambrian.

2. Geological setting

2.1. Paleogeography and section locations

The South China Block was located between ca. 5–20° N latitude during the Early Cambrian (Fig. 1A; Yang et al., 2015) and comprised the Yangtze and Cathaysia blocks (Fig. 1B; Li et al., 2008). The Yangtze Block consisted of an Archean-Paleoproterozoic crystalline basement and a sedimentary cover (Dong et al., 2011). The Yangtze Block experienced a gradual transition from a rift basin to a passive continental margin basin with the assembly of the Gondwana continent in the latest Neoproterozoic-early Paleozoic (Wang and Li, 2003). Four broad sedimentary facies belts dominate the Ediacaran-Early Cambrian Yangtze Block, comprising shallow-water shelf, intraplatform basin, slope and deep-water basin, as the water deepened from the northwest to the southeast on the passive continental margin (Fig. 1B; Jiang et al., 2012; Steiner et al., 2007; Yeasmin et al., 2017; Zhu et al., 2007). The lower Cambrian successions of the Upper Yangtze Block consist of the Maidiping Formation and the overlying Qiongzhusi Formation, in ascending order (Jin et al., 2016).

The studied Dongxihe section (32°38′30.36″N, N105°45′23.57″E) is located on the northeast margin of the Upper Yangtze intraplatform basin, ~5 km north of Yangmu town, Guangyuan City, Sichuan Province in Southwest China (Fig. 1B). The 65.04-m-thick exposure contains the Lower Cambrian Qiongzhusi Formation strata, predominantly deposited varying between a shallow shelf and deep-water shelf environment with the sea level rising and falling (Fig. 2). The Qiongzhusi Formation of the Dongxihe section is characterized by chert, shale and argillaceous siltstone shale in the Lower Member and alternating carbonaceous shale and cherty shale in the Middle Member (Fig. 2).

2.2. Stratigraphy of the Dongxihe section

Biostratigraphy of the Qiongzhusi Formation on the Yangtze Block has been well studied, for example, in the Meishucun section, Yunnan Province, and in the Maidiping section, Sichuan Province (e.g., Compston et al., 2008; Steiner et al., 2007; Zhu et al., 2019). Five assemblage zones have been reported for the Qiongzhusi Formation, including the poorly fossiliferous Interzone (Biozone IV), *Sinosachites flabelliformis-Tannuolina zhangwentangi* Assemblage Zone (Biozone V), *Pelagiella subtriangulata* Taxon Range Zone (BiozoneVI), *Parabadiella huio* Zone (Biozone VII) and *Wutanaspis-Eoredlichia* Interval Zone (Bizones VII) (Fig. 2; Compston et al., 2008; Steiner et al., 2007; Zhu et al., 2019). Approximate age constraints of the Qiongzhusi Formation in the Dongxihe section are provided by regional correlation along the Yangtze Block based on the previous lithostratigraphy, biostratigraphy and radiometric data. The poorly fossiliferous Interzone (Biozone IV), *Sinosachites flabelliformis-Tannuolina zhangwentangi* Assemblage Zone (Biozone V) recognized in the Lower and Middle Member of the Qiongzhusi Formation indicate a middle-late Xiaotanian Stage age (Fig. 2; Compston et al., 2008). The *Wutanaspis-Eoredlichia* Interval Zone (Bizones VII) in the Qiongzhusi Formation Upper Member belongs to an early-middle Qiongzhusian Stage age (Fig. 2; Compston et al., 2008; Steiner et al., 2007; Zhu et al., 2019). A SHRIMP U—Pb zircon age of 526.2 ± 1.9 Ma has been determined for a thin tuff from the base of the Qiongzhusi Formation in the Maidiping section of Leshan City Sichuan Province (Compston et al., 2008), consistent with a U—Pb zircon age of 526.5 ±
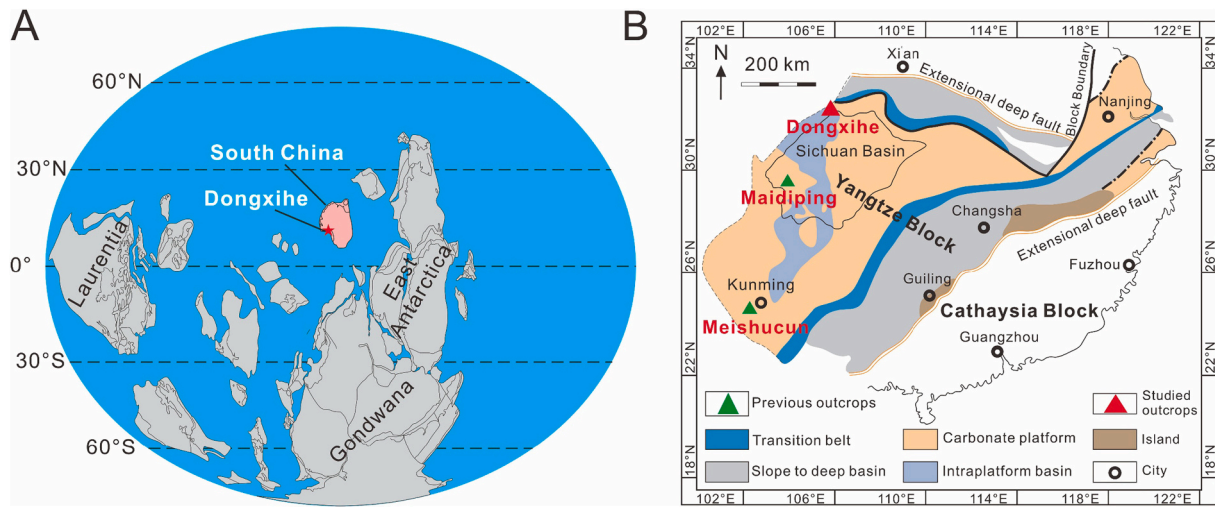
Fig. 1. (A) Global paleogeographic map in the Cambrian Age 3 (base map modified from Yang et al., 2015). Pink area: South China. Red star: Dongxihe section. (B) Paleogeographic map of South China in the Early Cambrian (Mou et al., 2012). Triangles: sections discussed in this study. (For interpretation of the references to colour in this figure legend, the reader is referred to the web version of this article.)

1.1 Ma for the bentonite from the base of the black shale succession at Meishucun, Yunnan Province (Fig. 2). The investigated successions at Dongxihe section covered the entire Lower Member and some of the Middle Member of Qiongzhusi Formation, corresponding to an approximate Stage 2 age (Fig. 2).

3. Materials and methods

3.1. Paleoclimate proxies

Geochemical data were measured at ca. 8-cm sampling intervals using portable X-ray Fluorescence spectroscopy (XRF: Thermo Scientific™ Niton™ XL3t Handheld XRF Analyzer) at the fresh rock surface along the studied section. A total of 814 geochemical data points were collected in the 'Geochemistry' mode of the instrument (50 kV beam energies). Individual analysis times were 60 s, consistent with recommendations for optimizing analysis times (e.g., Liu et al., 2021; Saker-Clark et al., 2019). In addition, cyclostratigraphic results of pXRF analysis are consistent with these conventional chemical methods, suggesting that robust cyclostratigraphy can be constructed using the portable X-ray instrument (Saker-Clark et al., 2019).

The geochemical components of marine sediment depend primarily on the supply of materials via physical erosion and chemical weathering (Jin et al., 2020, 2006). Thus, elemental variation in sedimentary rocks has been used to track climate Jin et al., 2006 during deposition (Calvert and Pedersen, 2007). XRF analysis of sedimentary rock has been widely employed for analysis and interpretation in cyclostratigraphy (e.g., Da Silva et al., 2019; Liu et al., 2021; Ruhl et al., 2016; Saker-Clark et al., 2019; Sinnesael et al., 2018). Aluminum (Al) is confined to the clay mineral fraction, whereas Zirconium (Zr) is concentrated in the heavy mineral zircon (i.e., ZrSiO4) (e.g., Fitzpatrick and Chittleborough, 2018; Taylor and McLennan, 1985; Zabel et al., 2001). Accordingly, high Zr/Al ratios might reflect preferential transport of heavy minerals during times of arid conditions and strong winds (e.g., Hofmann and Wagner, 2011; Rea et al., 1998; Zhang et al., 2015).

Magnetic susceptibility (MS) can indirectly characterize the concentrations and composition of magnetic minerals in sedimentary rock (Kodama and Hinnov, 2014). The MS value of marine sediments is affected by the terrigenous detrital mineral influx associated with the intensity of terrestrial weathering (e.g., Bloemendal and DeMenocal, 1989; Da Silva et al., 2013; Kodama and Hinnov, 2014) and diagenesis (e.g., Da Silva et al., 2013; Riquier et al., 2010). There is a linear correlation between MS and Al concentration as a proxy for the clay mineral

fraction ($R^2 = 0.63$; Fig. S1), indicating that MS values of the Dongxihe section are mainly determined by climate changes and are not significantly altered by diagenesis. MS variations of sedimentary rocks have been used as a proxy for detecting astronomically forced climate cycles (e.g., Ellwood et al., 2013; Hinnov, 2013; Li et al., 2019b; Omar et al., 2021; Wu et al., 2013a, 2013b). MS was measured at an average resolution of 2.0 cm using a handheld SM-30 MS instrument (ZH Instruments Ltd., Czech Republic) at the fresh rock surface along the Dongxihe section. The susceptibility sensitivity of SM-30 is 1×10^{-7} SI unit. A total of 3253 MS data points were measured along the Dongxihe section.

3.2. Time series analysis methods

The recognition and interpretation of potential astronomical-climate signals in the MS and Zr/Al records along the studied successions have been carried out following procedures in Li et al. (2019b): (1) all proxies (MS and Zr/Al records) were nonlinearly detrended by subtracting a 35% weighted average (Cleveland, 1979) to remove the long-term trend. (2) Evolutionary fast Fourier transform (eFFT) with a 10-m sliding window is utilized to inspect variable cycles and detection of variable changing accumulation rates (Fig. S2; Kodama and Hinnov, 2014). (3) Multi-taper method (MTM) power spectra of the detrended climate proxies were analyzed for the dominant frequency peaks against robust first-order autoregressive "AR(1)" red noise models (Mann and Lees, 1996). (4) The correlation coefficient (COCO) method evaluates the correlation coefficients between the power spectrum of the astronomical solution and that of the time-calibrated paleoclimate proxy series by testing a range of sediment accumulation rates (SAR) (Li et al., 2018). The SAR with the highest COCO probably and lowest null hypothesis (H_0, no orbital forcing) significance level represents the optimal SAR. Variable sediment accumulation rates through studied succession were tracked by the evolutionary correlation coefficient (eCOCO) method with a 10-m sliding window (Li et al., 2018). The optimal accumulation rate estimated by COCO (i.e., correlation coefficient) and eCOCO (evolutionary correlation coefficient) methods could test the veracity of our astronomical interpretation. (5) Gaussian bandpass filtering was utilized to isolate the signals of the Milankovitch components from the paleoclimate series in both the stratigraphic domain and time domain. (6) Floating astronomical timescale is constructed by tuning the long eccentricity-related sedimentary wavelengths to the 405 kyr cycles. All analysis steps were carried out using *Acycle v2.4.1* software (Li et al., 2019a).
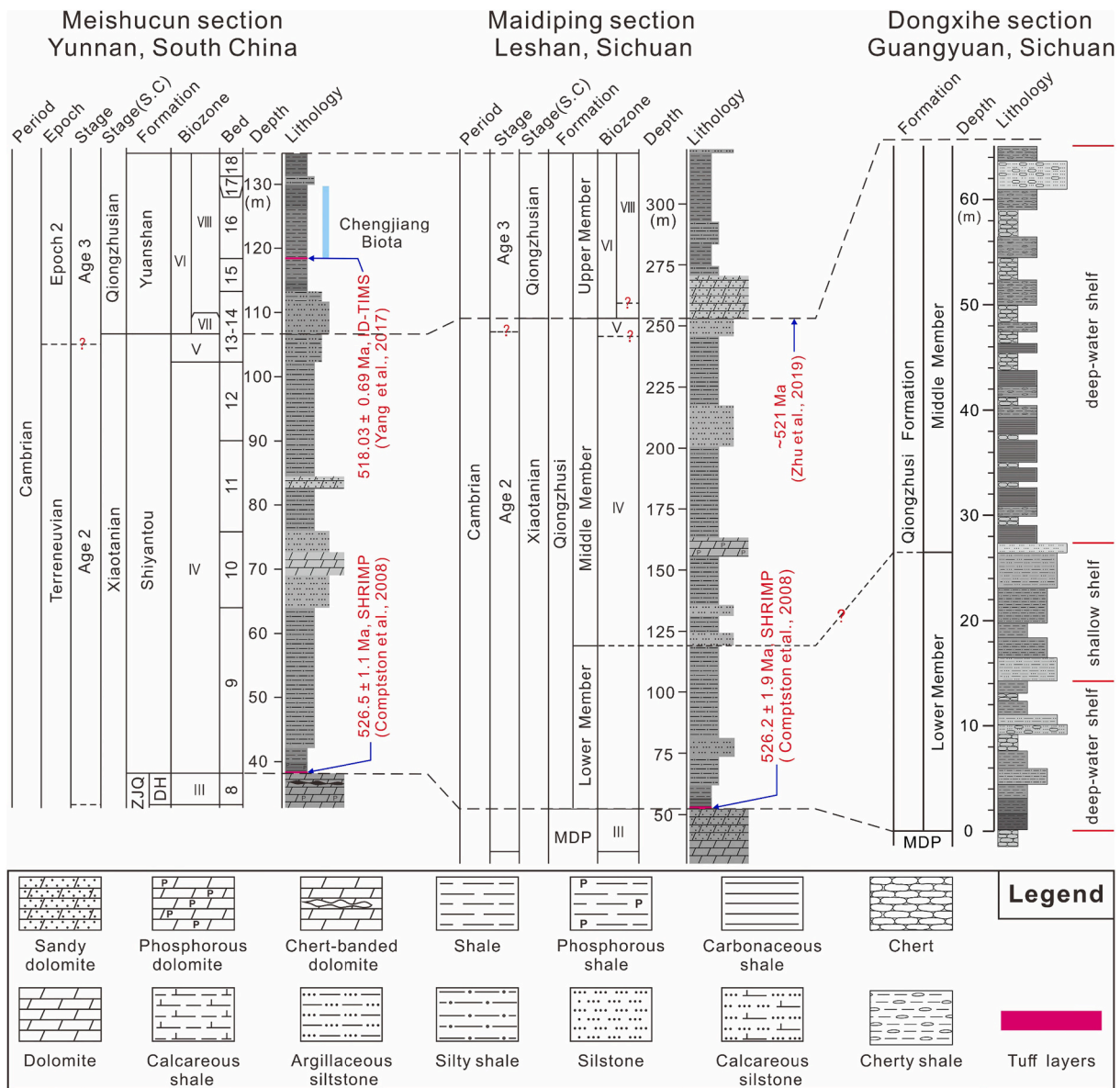
Fig. 2. Stratigraphic correlation of the Lower Cambrian successions in South China constrained by chronostratigraphy, biostratigraphy, and lithostratigraphy. The litho-stratigraphy, radiometric dates and bed numbers are based on Brasier et al. (1990), Compston et al. (2008) and Yang et al. (2018); bio-zones are from Brasier et al. (1990), Compston et al. (2008) and Steiner et al. (2007). Dashed black lines represent time equivalent horizons based on lithostratigraphy and biostratigraphy. Ashs beds are marked by red bars. Biozone III: *Watsonella crosbyi* Assemblage Zone, Biozone IV: Poorly fossiliferous interzone, Biozone V: *Sinosachites flabelliformis-Tannuolina zhangwentangi* Assemblage Zone, BiozoneVI: *Pelagiella subtriangulata* Taxon Range Zone, Biozone VII: *Parabadiella huio* Zone; Biozone VII: *Wutanaspis-Eoredlichia* Assemblage Zone; ZJQ: Zhujiaqing Formation, MDP: Maidiping Formation, CLP: Canglangpu Formation, DH: Daihai Member. (For interpretation of the references to colour in this figure legend, the reader is referred to the web version of this article.)

4. Results

4.1. Paleoclimate proxies

In the Dongxihe section, MS and Zr/Al values vary between 0.0092 $\times 10^{-3}$ SI and 0.1241 $\times 10^{-3}$ SI and from 0.14 $\times 10^{-3}$ to 13.50 $\times 10^{-3}$, respectively. Through the studied section, variations in the MS and Zr/Al series are broadly correlated with lithologic trends (Fig. 3). In the Qiongzhusi Lower Member, high MS and low Zr/Al values are typically associated with shale and chert clay-rich sediments, whereas lower MS and high Zr/Al values correspond to coarser-grained silty shale, cherty siltstone and siltstone (Fig. 3). However, in the Qiongzhusi Middle Member, high MS and low Zr/Al values generally correspond to chert, whereas low MS and high Zr/Al values are typically associated with cherty shale (Fig. 3). This discrepancy was probably attributed to

sedimentary facies change due to a relatively higher sea level during the deposition of Qiongzhusi Middle Member (Jin et al., 2016; Zhu et al., 2003).

4.2. Time series analysis

Spectral analysis of the untuned MS series displays significant peaks (>95% confidence level) at wavelengths of 5.91 m, 1.64 m, 0.43–0.40 m, and 0.30–0.24 m, respectively (Fig. 4A and C). The Zr/Al series show obvious cycles with wavelengths at 5.81 m, 1.37 m, 0.52–0.44 m, and 0.30–0.25 m, respectively (Fig. 4B and D). The ratios between these cycles are broadly consistent with those between the expected Milankovitch periods of the Early Cambrian long eccentricity (405 kyr), short eccentricity (~95 and ~ 130 kyr), obliquity (~32.3 kyr) and precession (~18 kyr) in the Waltham'm model (~523.5 Ma; Waltham, 2015).
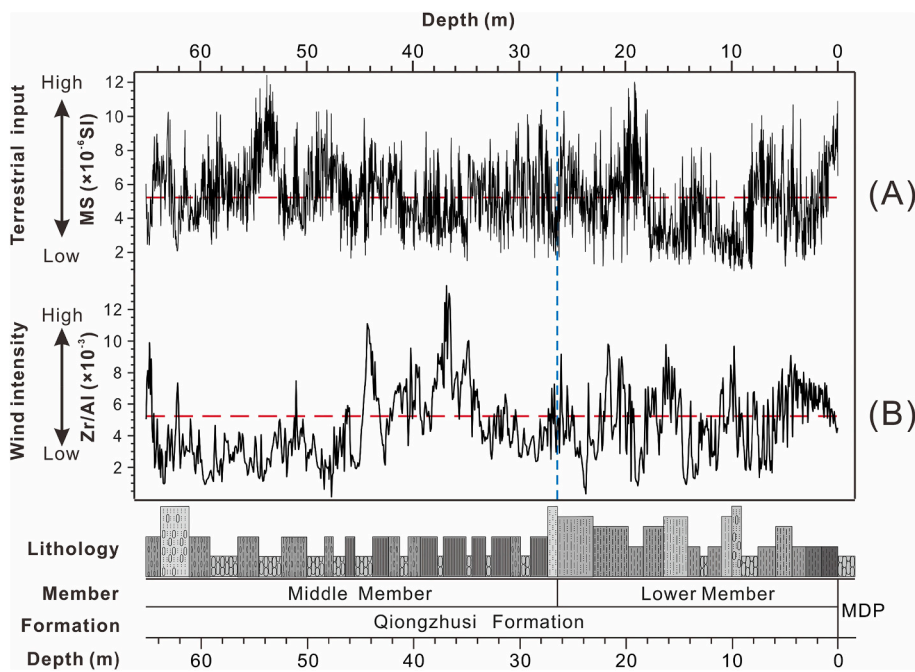
Fig. 3. Variations in paleoclimate proxies of the Early Cambrian Qiongzhusi Formation at Dongxihe section. (A) MS and (B) Zr/Al ratios. Dashed red lines represent the mean values of the corresponding time series. Vertical dashed blue line represents the boundary between the Lower Member and the Middle Member. MS and geochemical data were measured at 0.02 m and 0.08 m intervals, respectively. (For interpretation of the references to colour in this figure legend, the reader is referred to the web version of this article.)

The biostratigraphic and radiometric framework of the Dongxihe section can provide a broad duration of slightly <5.2 Myr for the 65.04-m thickness studied successions (Fig. 2; ~526.2 ± 1.9 Ma to ~521 Ma), yielding a mean sedimentation rate of slightly more than ~1.25 cm/kyr. The COCO and eCOCO analysis with 2000 Monte Carlo simulations were performed on tested sedimentation rates ranging from 0 to 4 cm/kyr to reveal the optimal sedimentation rate for the studied interval (Fig. 5). The COCO and eCOCO sedimentation rate maps of the MS and Zr/Al series reveal an average sedimentation rate of 1.2–1.9 cm/kyr, with a null hypothesis of no orbital forcing at a 99.9% confidence (Fig. 5 and Fig. S3). Taken together, we consider that the optimal mean sedimentation rate of the Qiongzhusi Fm of the Dongxihe section ranges between 1.2 and 1.9 cm/kyr. Based on the estimated average sedimentation rates of 1.2–1.9 cm/kyr, the ca. 6 m (5.91-m to 5.81-m) cycles probably represent the 405-kyr long eccentricity cycles. With this assumption, 1.64-m to 1.37-m cycles, 0.52-m to 0.40-m, and 0.30-m to 0.24-m cycles would represent ~100 kyr short eccentricity, ~32 kyr obliquity, and ~18 kyr precession cycles, respectively.

These ca. 6 m wavelengths in the MS and Zr/Al series are isolated using the Gaussian bandpass filtering (Fig. 4) and were attributed to the 405-kyr long-eccentricity cycles resulting in a ~ 5.0 Myr long floating astronomical time scale for the Qiongzhusi Formation at Dongxihe (Fig. 6 and Table S1). The MTM power spectra of the 405 kyr-tuned MS and Zr/Al series show significant peaks with periods of 924–963 kyr, 405 kyr, 130–90 kyr, 35.7–29.0 kyr and 19.4–16.7 kyr, all with confidence levels above 95%, while 128 kyr, 99 kyr, 20.5 kyr and 19.7 kyr are weakly expressed (Fig. 7). These periodicities are broadly consistent with the expected periods of Cambrian obliquity (~32.3 kyr) and precession (~18 kyr) in the Waltham'm model (~523.5 Ma, Waltham, 2015).

5. Discussion

5.1. The astronomical time scale for the early Cambrian Qiongzhusi Formation

The two obtained floating astronomical time scales (ATS) yield a duration of the studied interval in the Dongxihe section ranging from 4.99 Myr (MS) to 5.00 Myr (Zr/Al). These floating astrochronologies are in good agreement with each other and result in an average duration of 5.0 Myr for the studied succession. The absolute astronomical time was constructed by anchoring the floating ATS derived from the MS series to the base age of the Qiongzhusi Formation to 526.2 ± 1.9 Ma (Compston et al., 2008).

Our age model has at least two major sources of uncertainty: (1) uncertainty of 1.90 Ma (1σ) from the SHRIMP U—Pb dating for the tuff at the base Qiongzhusi Formation, and (2) the uncertainty of 0.2 Myr derived from floating ATS. An uncertainty of our floating astrochronology without astronomical solutions is estimated to be ~0.2 Myr (half of a long eccentricity period), which is derived from the 405 kyr band pass filtering uncertainty considering unsteady sedimentation rates and non-linear climate response to eccentricity forcing (e.g., Sinnesael et al., 2019). Thus, we follow previous studies (e.g., Da Silva et al., 2020) and consider the two sources of uncertainty resulting in total uncertainty of 1.91 Myr (obtained from $\sqrt{1.90^2 + 0.2^2}$, where 1.90 Myr represents the uncertainty of the SHRIMP radio-isotopic dating and 0.2 Myr is the uncertainty of floating ATS) for our absolute ATS. Besides, sedimentology and the shifting phase of proxies relative to orbital changes may also be potential sources of uncertainty (e.g., Sinnesael et al., 2019), but straightforward quantification of these uncertainties is challenging. A more conservative estimate of the dating error is to add up both uncertainties, thus 2.1 Myr. Future precise ages (e.g., CA-ID-TIMS U—Pb ages) should be used to update this calculation. The studied interval is probably deposited from 526.2 ± 1.91 Ma to 521.23 ± 1.91 Ma (Fig. 6), indicating that the investigated succession falls into Cambrian Age 2, consistent with those derived from biostratigraphy and radiometric dating (Compston et al., 2008; Steiner et al., 2007; Zhu et al., 2019). Consequently, the base age of the Middle Member is constrained at 524.16 ± 1.94 Ma (Fig. 6), consistent with astrochronological constraints reported by Zhang et al. (2022). The sedimentation rate curves derived from recognized 405-kyr cycles in the MS and Zr/Al series are partly relying on the objective sedimentation rate map of eCOCO analysis (Fig. 5D), supporting our cyclostratigraphic interpretation.

5.2. Astronomically forced ITCZ migration dynamics

The paleogeographic location of the Dongxihe record was considered close to the northern tropics between ca. 5°N and 20°N latitude during
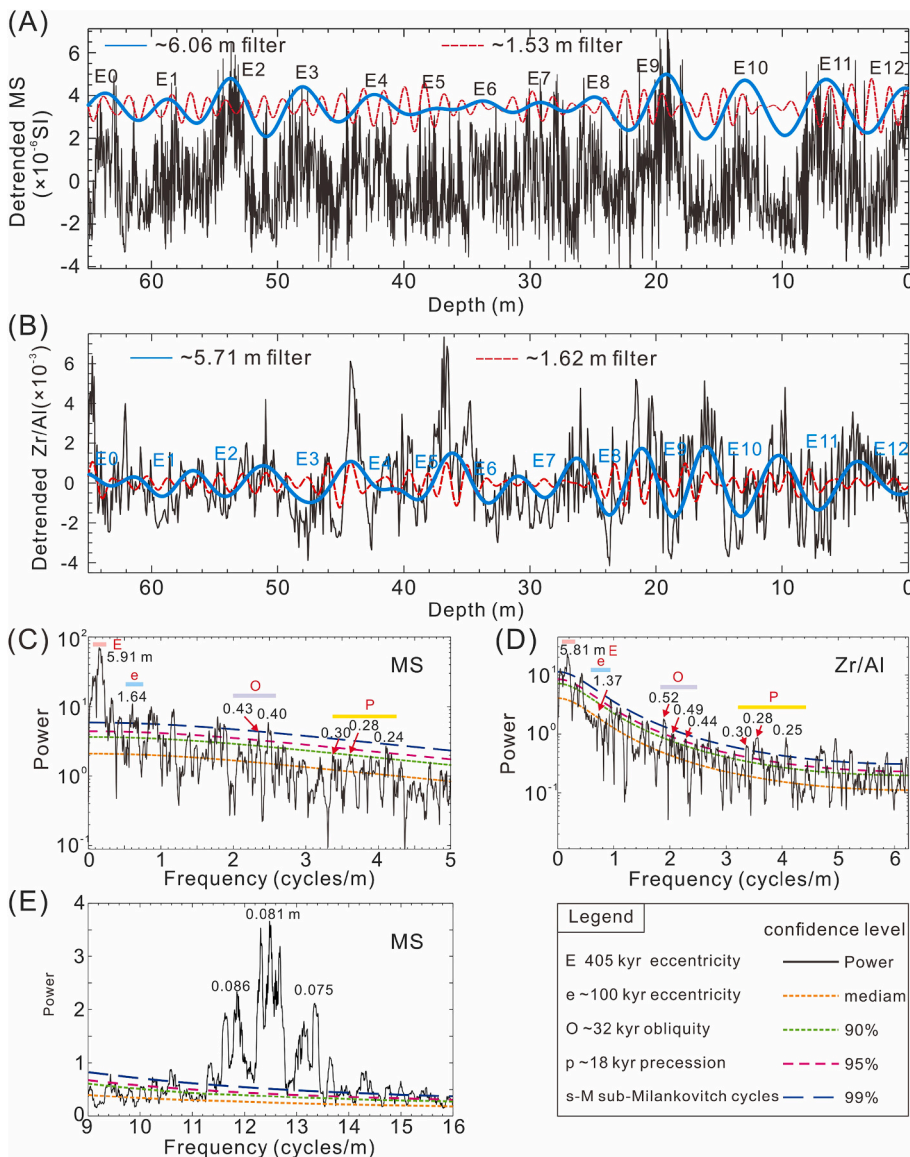
Fig. 4. Detrended paleoclimate proxies after removing a 35% 'lowess' trend and the interpreted long- (thick blue, 405 kyr) and short-eccentricity (dotted red, ~100 kyr) cycles and their corresponding MTM power spectrum with confidence levels. (A) Detrended MS and filtered 6.06-m and 1.53-m wavelengths (Gaussian filter, passband: 0.165 ± 0.055 and 0.65 ± 0.13 cycles/m, respectively), (B) Detrended Zr/Al and filtered 5.71-m and 1.62-m wavelengths (Gaussian filter, passband: 0.175 ± 0.035 and 0.615 ± 0.135 cycles/m, respectively). (C, D) 2π Multi-taper method (MTM) power spectra of MS and Zr/Al series in (A) and (B), respectively. (E) 3π MTM power spectrum of MS series highlights sub-Milankovitch cycles, shown with the robust first-order autoregressive "AR(1)" red noise models (Mann and Lees, 1996). Significant peaks are labeled in meters. (For interpretation of the references to colour in this figure legend, the reader is referred to the web version of this article.)

the Early Cambrian Age 2-Age 3 (Fig. 1; Yang et al., 2015). According to the understanding of the present atmospheric circulation model, this paleogeographic location probably exposed the Qiongzhusi Formation directly to the ITCZ-related paleo-Hadley Cell dynamics (e.g., Hofmann and Wagner, 2011; Mamalakis et al., 2021; Wagner et al., 2013). The MTM power spectra of the 405-kyr tuned MS and Zr/Al series display significant 405 kyr long eccentricity, ~130–90 kyr short eccentricity, ~29 kyr obliquity and ~ 18 kyr precession cycles (Fig. 7), suggesting a strong correlation between periodic variations in the MS and Zr/Al series and the orbital-paced solar insolation variations. Thus, quasi-periodic fluctuations in the MS and Zr/Al series could be interpreted as alternations between wet and dry cycles, resulting from changes in monsoon intensity and trade wind pattern under the ITCZ-related paleo-Hadley Cell dynamics induced by orbital-forced insolation variations.

The modern Indian Ocean and Western Pacific warm pool with maximal solar heating and sea surface temperature provides the most intensive latent heat and moisture from the ocean to the atmosphere and witness the largest ITCZ displacement in the annual cycle (e.g., Pierrehumbert, 2000; Wang et al., 2014). Currently, the ITCZ shifts between 9°N in boreal summer and 2°N in boreal winter over the central Atlantic and Pacific oceans. The ITCZ migrates more sharply over the Indian Ocean and adjacent land surface between a mean latitude of 20°N in the

Northern Hemisphere summer and 8°S in the Northern Hemisphere winter, contributing to the seasonal rainfall variability of the South Asian monsoon (Gadgil, 2003). The approximate location of the Early Cambrian ITCZ is schematically illustrated by analogy with the present global atmospheric climate model (Fig. 8A). During the Northern Hemispheric summer, a strong South China low-pressure cell could occur due to local land-ocean thermal contrasts and thus drive the ITCZ across the South China block. Therefore, the Dongxihe region could suffer from intense convective clouds and intensified monsoon precipitation under such a configuration (e.g., Liu et al., 2015; Philander et al., 1996; Waliser and Gautier, 1993). In the Northern Hemispheric winter, the ITCZ is likely located in the Southern Hemisphere tropics due to the relatively warming southern hemisphere. This could leave the South China block far away from the rain belt of the ITCZ and under the enhanced influence of the dry northeasterly trade winds. The Cariaco basin, located in Venezuela with a paleolatitude of ca. 10° N, provides clear evidence for a similar mechanism that drives the seasonal migration of the ITCZ (Haug et al., 2001; Peterson et al., 2000). The ITCZ is overhead on the Cariaco basin during the summer, the monsoon rainfall is maximum, and trade winds are weak. As the ITCZ moved southwards in winter, the trade winds intensified, and the hydrological cycle in the Cariaco basin weakened.
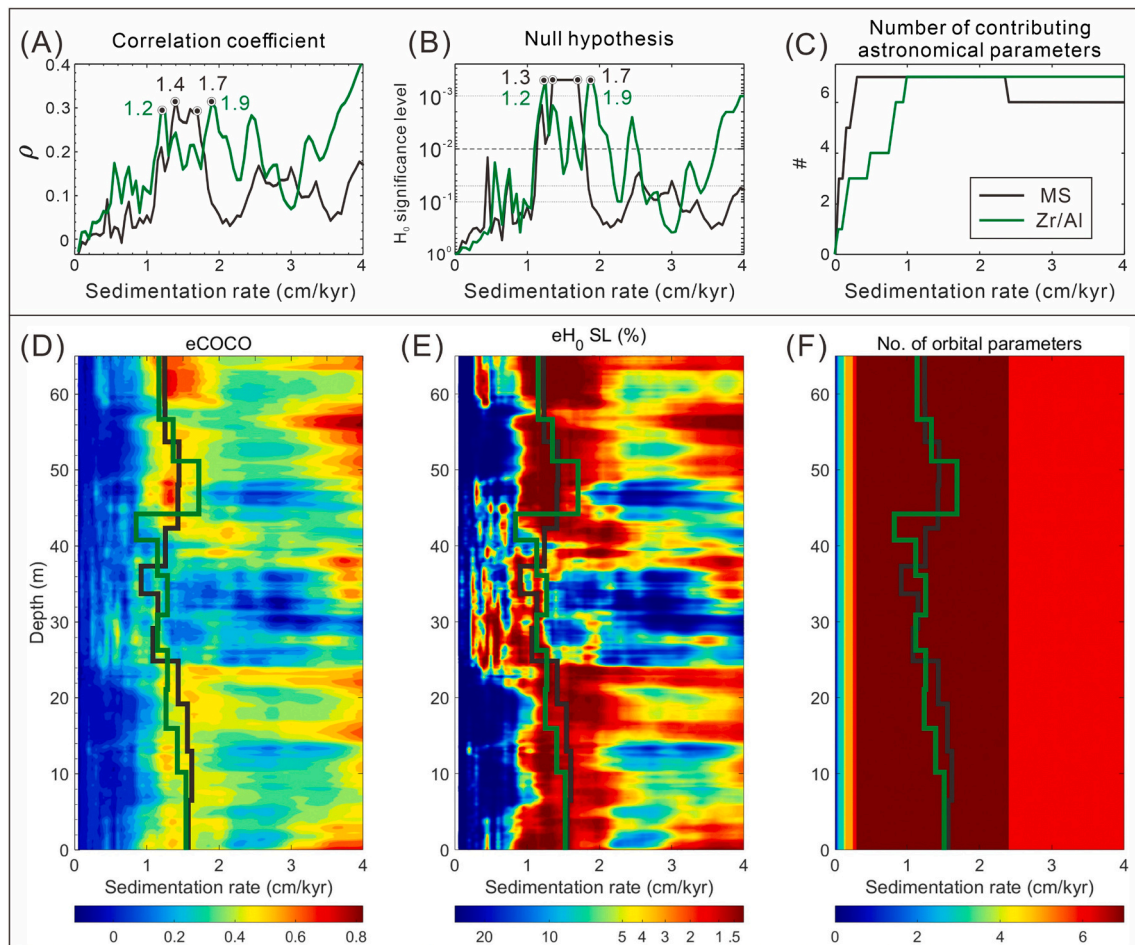
Fig. 5. COCO and eCOCO sedimentation rate map of MS (black line) and Zr/Al (green line) series. For both the COCO and eCOCO analysis, test sedimentation rates range from 0 to 4 cm/kyr with a step of 0.05 cm/kyr, and the number of Monte Carlo simulations is 2000. For eCOCO analysis of MS series, the sliding window is 10 m, with a sliding window step of 0.2 m. (A) Correlation coefficient between the power spectra of target astronomical solution and MS and Zr/Al series. (B) Null hypothesis significance levels. (C) Number of contributing astronomical parameters. (D) eCOCO sedimentation rate map shown with sedimentation rate curves derived from the recognized 405-kyr cycles of the MS (black line) and Zr/Al series (green line). (E) Evolutionary null hypothesis (H_0) significance level. (F) Evolutionary map of the number of contributing astronomical parameters. (For interpretation of the references to colour in this figure legend, the reader is referred to the web version of this article.)

We note that, on the eccentricity scale, periods of eccentricity maxima are primarily characterized by intervals with higher MS and lower Zr/Al values, which likely indicates relatively wetter conditions in summers (e.g., Zhang et al., 2022; Fig. 6). In contrast, periods of eccentricity minimum are mainly associated with intervals of lower MS and higher Zr/Al values (e.g., Zhang et al., 2022; Fig. 6), suggesting relatively dry conditions. Generally, the direct effect of eccentricity on solar insolation is negligible (e.g., Clemens and Tiedemann, 1997; Paillard, 2010); however, the eccentricity cycle can affect the Earth's climate system significantly via modulating the amplitude of climatic precession (Abels et al., 2010; Crowley et al., 1992; Short et al., 1991). During eccentricity maxima, extreme precession can be responsible for seasonal insolation differences of around 20% (Abels et al., 2013; Laskar et al., 2004; Valero et al., 2016). Distinct insolation variations dominated by the precession cycle at the time of eccentricity maximum might push a more significant northward/southward displacement of the ITCZ and subsequent covariation of the position of the ancient Hadley Cell (e. g., Cai et al., 2012; Schneider et al., 2014; Wang et al., 2017). In turn, these large meridional shifts of the ancient Hadley Cell leave distinct contrast in monsoonal precipitation and trade wind patterns and thus result in clear wet-dry cycles and seasonal contrast, as evidenced by periodic variation in the MS and Zr/Al series at Dongxihe.

When eccentricity reached its maxima and the northern hemisphere

summer resides at perihelion, the amount of insolation received by the northern subtropics may have increased significantly. An intensified cross-hemispherical pressure contrast between the continental low-pressure cell and the subtropical high-pressure cell in response to precession-dominated additional Northern Hemisphere summer insolation could push a northward shift of the ITCZ relative to the "normal" Northern Hemisphere summer (e.g., De Vleeschouwer et al., 2012; Liu et al., 2015; Schneider et al., 2014). Consequently, an intensified meridional thermal-pressure gradient could enhance monsoon intensity and increase moisture transport towards the continent, resulting in an intense hydrological cycle at Dongxihe. Under such climatic context, increased continental detrital sediment flux and decreased aeolian dust delivery to the ocean would occur, in agreement with the observed higher MS and lowered Zr/Al values at Dongxihe during precession maximum (Fig. 6). Strong paleoclimate evidence from Asia and America over the past ~200 kyr suggested that changes in the extent of the Hadley Cell are intensely controlled by precession cycles (Wang et al., 2004, 2008). Furthermore, a similar climate forcing mechanism was proposed to interpret monsoon-like circulation in eastern Euramerica associated with ITCZ-related dynamics during the Mid-Devonian (De Vleeschouwer et al., 2012). Thus, ITCZ-related dynamics governed by the amount of insolation associated with precession cycles is likely one of the primary drivers of low-latitude climate change during the Early
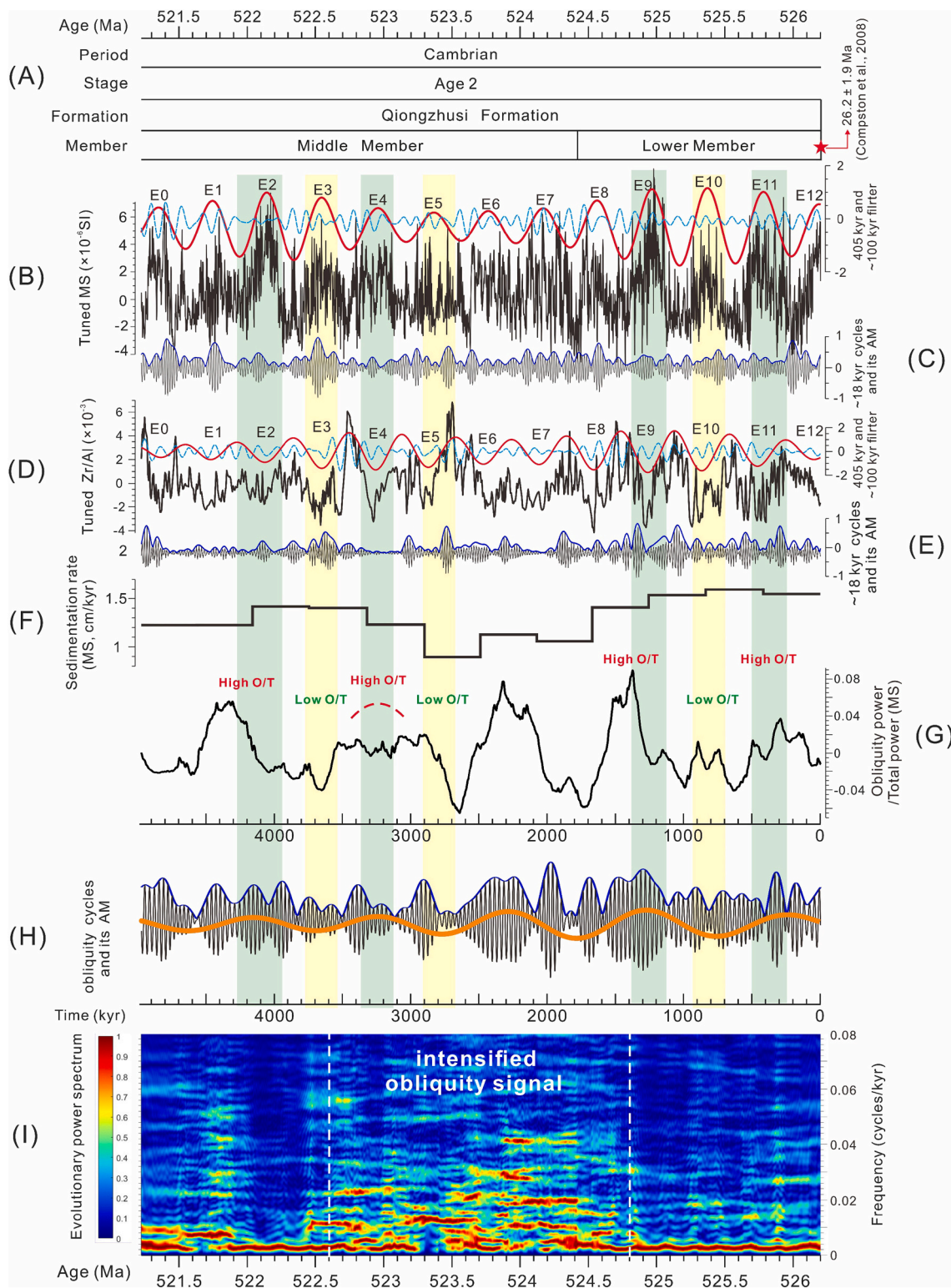
Fig. 6. Long eccentricity cycle-tuned time series of the Dongxihe section. (A) Chronostratigraphy of the Early Cambrian Qiongzhusi Formation. (B, D) Tuned MS and Zr/Al plotted with their filtered 405-kyr (red line, Gaussian filter, both passband: 0.00247 ± 0.0005 cycles/kyr) and ~ 100-kyr cycles (dashed blue line, Gaussian filter, both passband: 0.00895 ± 0.00205 cycles/kyr). (C, E) Filtered ~18 kyr precession cycles (black line) and their amplitude modulation (dark blue line) were obtained by Hilbert Transform (both passband: 0.0555 ± 0.0095 cycles/kyr) of the tuned MS and Zr/Al series. (F) Sedimentation rate curve derived from the recognized 405-kyr cycles of the MS series. (G) Obliquity power/total power was integrated with paired frequency bands of 1/37–1/28 cycles/kyr from the tuned MS series, and the total power was integrated from frequency 0 to 0.08 cycles/kyr with a 500-kyr sliding window. (H) Amplitude modulation (AM) envelope (dark blue line) of obliquity cycles was determined by the Hilbert Transform of obliquity cycles (black line; bandpass: 0.0031 ± 0.0005 cycles/kyr) from the tuned MS series and filtered ~1.0 Myr AM cycles (orange line; Gaussian filter; bandpass: 0.001 ± 0.0002 cycles/kyr). (I) Evolutionary power spectrum of the tuned MS series was calculated using a 500-kyr sliding window and a 5-kyr sliding step. Yellow and green bars denote high-obliquity-high-eccentricity, and high-obliquity-low-eccentricity intervals, respectively. (For interpretation of the references to colour in this figure legend, the reader is referred to the web version of this article.)
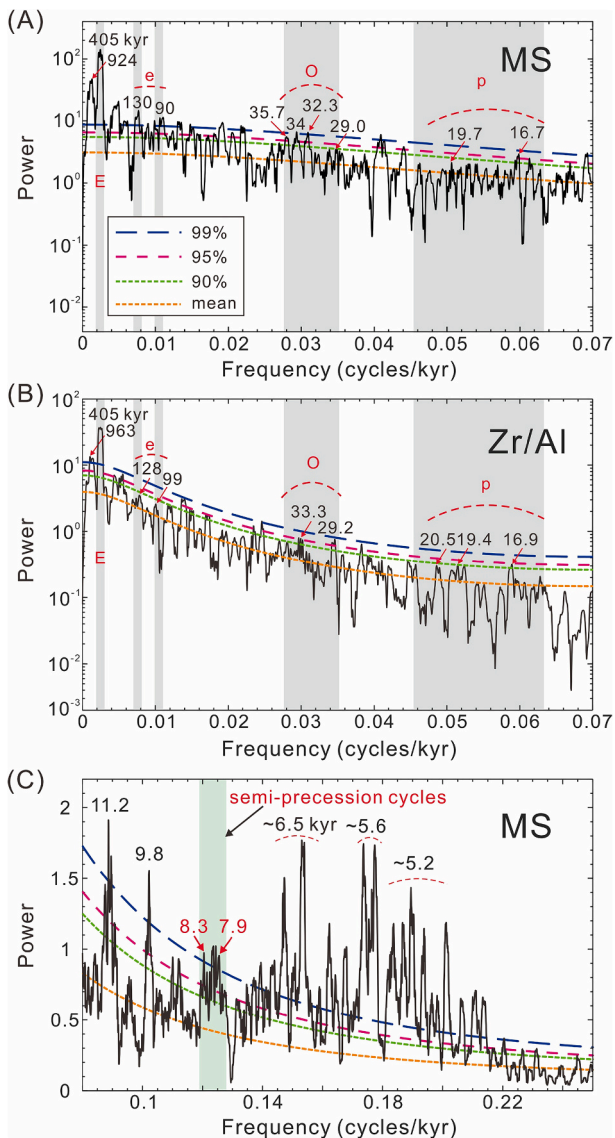
Fig. 7. 2π Multi-taper method (MTM) power spectra of the tuned MS (A, C) and Zr/Al (B), against robust first-order autoregressive "AR(1)" red noise models (Mann and Lees, 1996). Grey bars in panels (A and B) represent the expected astronomical frequencies at 523.5 Ma in the Waltham's model (Waltham, 2015). Green bar in panel C represents potential semi-precession periods for the Early Cambrian. (For interpretation of the references to colour in this figure legend, the reader is referred to the web version of this article.)

Cambrian.

The obliquity power intensity and amplitude modulation in the paleoclimate proxy are evaluated by both the ratio of obliquity variance to the total variance (O/T) and the Hilbert transform method (Figs. 6 and 10). The O/T approach is appropriate because this method can overcome the effect of the lithology change, which could lead to major amplitude variations not related to orbital forcing. We note that periods of high eccentricity and high obliquity are mainly characterized by higher MS and lower Zr/Al values (Fig. 6; green bars) relative to the scenarios with high eccentricity and low obliquity (Fig. 6; yellow bars), indicating an enhanced monsoonal circulation. This highlights the important role of obliquity forcing in modulating monsoonal precipitation at Dongxihe. Obliquity forcing is expected to dominate poleward transportation of heat and moisture through control of the meridional insolation gradient and cross-equatorial pressure/thermal gradient and thus make an influence on low-latitude climate processes (Fig. 8B; e.g.,

Heitmann et al., 2017; Li et al., 2016; Liu et al., 2015; Prell and Kutzbach, 1992). At high eccentricity and high obliquity, a stronger cross-equatorial pressure contrast between an enhanced Southern Hemisphere Gondwana high and South China low strengthens the northward shift of the ITCZ rain belt to its northernmost position in boreal summer (Fig. 8C). Besides, the extended Gondwana continent in the southern hemisphere extending to the South Pole during the Early Cambrian could have further strengthened the cross-equatorial pressure gradient (orographically thermal forcing). This northward migration of the ITCZ would increase precipitation in South China in boreal summer. For the scenario with high eccentricity and low obliquity, the cross-equatorial pressure gradient is not as strong as compared to high-precession and high-obliquity cases, and the ITCZ rain belt moved southern (Fig. 8D). Consequently, Dongxihe experienced relatively reduced monsoonal rainfall during those periods.

Evolutionary power spectrum of the 405 kyr tuned MS series in our section displays a relatively intensified obliquity signal in the interval of ~524.8 – ~522.6 Ma (Fig. 8H). Zhang et al. (2022) reported an increase in obliquity power in gamma-ray logs from the Qiongzhusi Formation in South China during the ~525- ~ 523 Ma interval. This intensified obliquity signal likely reflects more sensitivity of low-latitude climate processes responding dynamically to high-latitude obliquity forcing (e. g., Levy et al., 2019; Wang et al., 2021). For example, the obliquity signal in Pliocene benthic foraminiferal $\delta^{18}O$ records increased significantly with the advance of the Antarctic marine ice sheet at ~24- ~ 19 Ma (Lear et al., 2008). Besides, low chemical index of alteration (with an average value of ~65) and elevated Ti/Al values characterize the middle Jiumenchong Formation (roughly equivalent to the Qiongzhusi Formation), suggesting that a short-term, relatively cold and arid climate event probably occurred on the Yangtze Block during the Early Cambrian (Zhai et al., 2018). We infer that circumpolar current, global sea level and heat transport variations, associated with the episodic development of the Antarctic ice sheet under an Early Cambrian greenhouse lacking permanent ice sheets (e.g., Hearing et al., 2018; Wotte et al., 2019), probably led to this enhanced obliquity signal via altering cross-equatorial pressure/thermal gradient (e.g., Heitmann et al., 2017; Levy et al., 2019; Liu et al., 2015; Wang et al., 2021). However, Bosmans et al. (2015) argued that without high-latitude ice sheet fluctuation, obliquity signals could occur in low-latitude climate in relation to tropical circulation dynamics associated with obliquity-induced changes in the trans-equatorial insolation gradient. Alternative scenarios also exist; for example, the enhanced obliquity signal is likely attributed to the better preservation of the obliquity signal under a decrease in sedimentation rates (e.g., Wang et al., 2021). In fact, intervals of high obliquity are not characterized by relatively low sedimentation rates during the intensified obliquity from ~524.8 to 522.6 Ma (Fig. 6F and G). In addition, if the increase in obliquity power at ~524.8–522.6 Ma interval was related to a decrease in sedimentation rate, the time interval should not be ~524.1 Ma to 523.5 Ma and 523.1–522.8 Ma, but would be ~524.5 Ma to 524.2 Ma and 523.6 to 523.3 Ma (Fig. 6F, G and H). As a result, we favor the first interpretation. By contrast, the obliquity signal throughout the Zr/Al series is weaker than those in the MS series (Fig. S4; see supplementary information, SI). An interpretation for this weakened obliquity signal is likely due to a weaker sensitivity of Zr/Al to high-latitude obliquity forcing.

Taken together, the obliquity signal in our records indicates that precession forcing is not the only orbital forcing mechanism operating on the ITCZ movement in the Early Cambrian low-latitude tropics and that obliquity cycles in tandem with precession forcing can shift the position of the ITCZ. The tropical precipitation variations in Papua New Guinea, located at the southern border of the ITCZ over the past 282 kyr have been broadly attributed to the meridional migration of the ITCZ position induced by combined precession and obliquity changes (Liu et al., 2015). Due to the lack of specific details of summer insolation variability in the Northern Hemisphere during the Early Cambrian, more clear details of the migration of ITCZ position responding to orbital-
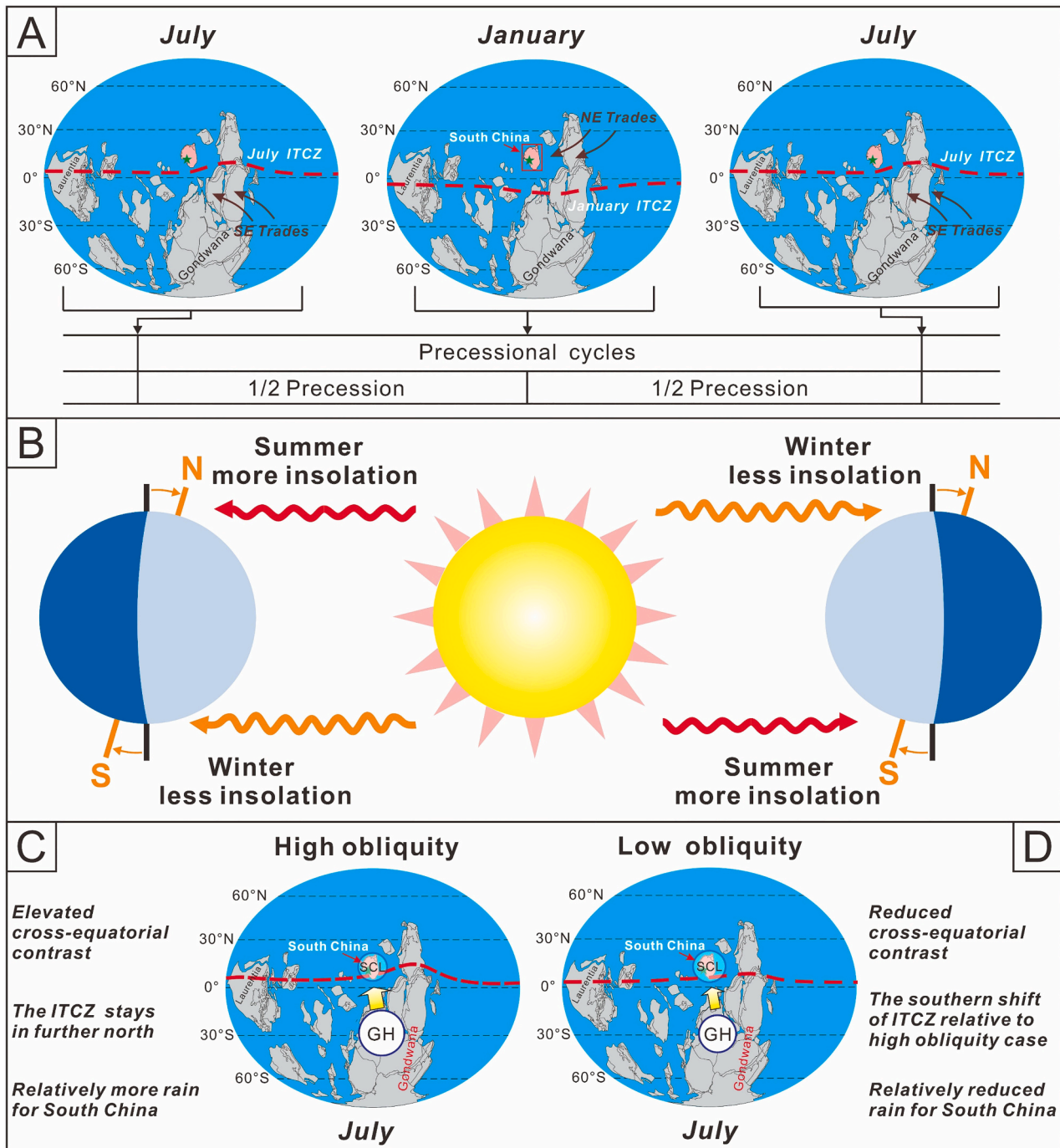
Fig. 8. (A) Conceptual model of paleoclimate changes showing the location of the intertropical convergence zone (ITCZ) during the Early Cambrian (paleogeographic map from Yang et al., 2015). Red dotted line denotes inferred position of the Early Cambrian ITCZ. Brown arrows indicate important trade winds. (B) Illustration of variations in tilt angle modulating global average insolation, especially in high latitudes. (C, D) Schematic illustration of the response of the northern summer ITCZ position to changes in the cross-equatorial gradient. This illustration is based on high summer insolation conditions in the Northern Hemisphere (i.e., high eccentricity and high precession). (C) High obliquity and (D) Low obliquity. Green star represents the approximate location of the Dongxihe section. SCL: South China low; GH: Gondwana high. (For interpretation of the references to colour in this figure legend, the reader is referred to the web version of this article.)

induced insolation variations in deep time remains currently an outstanding challenge. Since our interpretations are mainly based on multiple paleoclimate proxies from one section, additional uncertainties, such as possible erosion and minor unconformity, may have been ignored. Therefore, different (independent) climatic proxies from contemporaneous sections and the application of climate models for data model comparisons are required to further validate the dynamics of Cambrian low-latitude climate change. Our study highlights

teleconnections between high-latitude obliquity forcing and low-latitude climate dynamics and paves a new path for deciphering the dynamics of Earth's climate in deep time.

5.3. Sub-Milankovitch cycles

It is classically advised that to observe a cycle through spectral analysis, at least four samples by cycle should be considered (e.g.,

Kodama and Hinnov, 2014; Martinez et al., 2016). Theoretically, our MS data of the Qiongzhusi Formation recorded at 0.02 m intervals can resolve the shortest oscillation wavelength of ~0.08 m at significance levels (Martinez et al., 2016), corresponding to ~6.1 kyr cycles according to the average sedimentation rate of ~1.3 cm/kyr derived from our interpretation. This enables the detection of ~12 kyr to ~6 kyr cycles at the high frequency end of the spectrum in tropical sediments of the Early Cambrian Qiongzhusi Formation. The MTM power spectrum of the untuned MS series displays obvious cycles with wavelengths at 0.086–0.075 m above the 99% confidence level (Fig. 4E). The MTM power spectrum of the 405 kyr tuned MS series shows peaks at 9.8–11.2 kyr and 8.3–7.9 kyr in the sub-Milankovitch frequency band (<12 kyr) (Fig. 7C). The 5.2–6.5 kyr cycles are beyond the shortest period that our data can resolve at significance levels; thus, we will not discuss these cycles.

In order to explore the astronomic origin of the observed cycles, amplitude modulation (AM) analysis of sub-Milankovitch cycles is conducted (Hinnov, 2000). AM envelope curves are obtained from the sub-Milankovitch period (~11 kyr and ~8 kyr cycles) signals extracted from the 405 kyr tuned MS series by Taner bandpass filters (Fig. 9A and B). The MTM power spectrum of the ~11 kyr AM series displays obvious peaks at ~1 Myr, ~410 kyr, ~100–85 kyr, and 55–40 kyr (Fig. 9C). The MTM power spectrum of ~8 kyr AM series displays obvious peaks at ~1.0 Myr, ~370 kyr, ~142- ~ 100 kyr, 77 kyr and 44 kyr (Fig. 9D). These results suggest that the ~11 kyr and ~ 8 kyr cycles are modulated by the ~100-kyr short eccentricity and 405-kyr long eccentricity, as well as ~1 Myr cycle, confirming the astronomic origin of the observed sub-Milankovitch cycles in the Qiongzhusi Formation.

There are significant 123 kyr, 95 kyr, 11 kyr, and 5.5 kyr cycles that are directly associated with eccentricity and harmonics of precession in

the amplitude of the seasonal cycle of energy received from the Sun in the modern equatorial (and, to a lesser extent, tropical) regions (Berger et al., 2006). Because the Sun passes directly overhead at both equinoxes in the modern tropics, the maximum insolation occurs twice in every precession cycle (~20 kyr), leading to an equatorial annual maximum insolation cycle of ~10 kyr (semi-precession cycle; Ashkenazy and Gildor, 2008; Berger et al., 2006; Crowley et al., 1992). Previous studies have demonstrated that the semi-precession cycles have periodicities of ~11 kyr to ~12 kyr during the Early Neogene to the Quaternary (e.g., Fox et al., 2017; Sun and Huang, 2006; Ulfers et al., 2022; Verschuren et al., 2009), of ~10 kyr during the Late Jurassic to the Middle Triassic (e.g., Boulila et al., 2010; Chu et al., 2020; Whiteside et al., 2011) and of ~7.7 kyr to ~8.5 kyr in the Mid-Devonian (e.g., Da Silva et al., 2019; De Vleeschouwer et al., 2012). Theoretically, the precession period would be gradually longer through time (from Paleozoic to Cenozoic) due to tidal dissipation; thereby, so would the semi-precession cycles (Berger et al., 1992; Berger and Loutre, 2009; Laskar et al., 2004; Williams, 2000). Paleoclimate archives across the Early Cambrian to the Late Cambrian have revealed periods of ~16 – ~20 kyr on precession cycles, consistent with those in our study (Fig. 7; e.g., Fang et al., 2020; Sørensen et al., 2020; Zhang et al., 2022; Zhao et al., 2022). Taken together, the ~7.9-kyr to 8.3-kyr cycles in the Early Cambrian Qiongzhusi MS series (~526–522.7 Ma) most likely correspond to semi-precession.

These semi-precessional cycles might be an essential characteristic response of the Early Cambrian tropical climate processes to orbitally-paced changes in solar insolation, reconciling with the paleogeographical location of South China near the equator (Yang et al., 2015). Besides, this halving of the precession cycle has also been noted in mid-latitude sediments (e.g., Ferretti et al., 2015; Sun and Huang, 2006; Zhang et al., 2019), even high-latitude ice cores (e.g., Mayewski et al., 1997), suggesting modulation of millennial-scale solar radiation changes in the tropics on mid- and high-latitude climate variability. A possible mechanism is that heat and moisture derived from warm ocean pools heated by tropical solar radiation, analog to the present western Pacific warm pool, is advectively transported to mid-and high-latitudes through the coupling of atmospheric and/or oceanic circulation (Crowley et al., 1992; Ferretti et al., 2015; Short et al., 1991). Further, the identification of an 11-kyr cycle in a mid-latitude climate archive during the Mi-1 deglaciation further supports this suggestion (Fox et al., 2017). Examinations of the multiple marine and terrestrial proxy records from Greenland and the Eastern Mediterranean in the early/middle Pleistocene to the present indicate that the intensity of half-precession (HP) weakened with increasing distance from the equatorial region; for example, HP signals in the North Atlantic are weaker, while a stronger signature occurs in the Eastern Mediterranean region (Ulfers et al., 2022).

The Dongxihe region in South China might experience a bimodal seasonal precipitation pattern during the Early Cambrian, which is associated with the twice-annual passage of the ITCZ induced by the intensity of semi-precession-related insolation variability, as is the case in monsoon rainfall variability from equatorial East Africa over the past 25,000 years (Verschuren et al., 2009). As a result, a doubled frequency of alternating wet and dry cycles driven by semi-precession cycles is expected. The biogeographic provinces of Late Triassic Pangea *traversodont cynodont* assemblages, which are restricted to a 6° equatorial swath (Whiteside et al., 2011), are suggested to be driven by the bimodal rainfall pattern associated with the semi-precession climatic cycle. A clear manifestation of ~7 kyr cycle in tropical sediments of the Qiongzhusi Formation confirms that the semi-precession cycle may significantly affect millennial-scale tropical climate patterns, as observed dynamics of millennial-scale climate change in regions near the equator during the Cenozoic and Mesozoic (Cramer et al., 2003; Jian et al., 2020; Ulfers et al., 2022; Verschuren et al., 2009; Whiteside et al., 2011), even during the Devonian to the Permian (Anderson, 2011; Da Silva et al., 2019; De Vleeschouwer et al., 2012; Elrick and Hinnov,
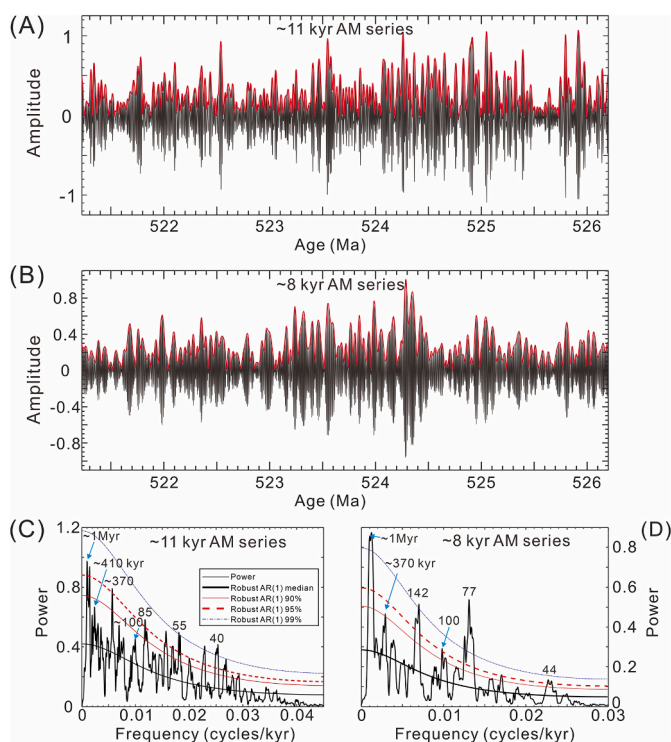

Fig. 9. Amplitude modulation (AM) of sub-Milankovitch cycles (i.e., ~11 kyr and ~ 8 kyr cycles, black line) was obtained from the 405-kyr-tuned MS series. (A, B) Amplitude modulation (AM) envelop curves (red line) were determined by the Hilbert Transform of bandpass-filtered ~11 kyr and ~ 8 kyr cycles (black line; bandpass: 0.09 ± 0.02 cycles/kyr and 0.124 ± 0.016 cycles/kyr, respectively). (C, D) 2π MTM power spectra of AM envelop curves of ~11 kyr and ~ 8 kyr cycles. (For interpretation of the references to colour in this figure legend, the reader is referred to the web version of this article.)

2007; Sinnesael et al., 2021). In any case, this study provides information on how orbitally induced insolation changes modulated millennial-scale tropic climate variability in deep time.

5.4. Chaotic behavior of the Solar System in the early Paleozoic

Power spectra of both tuned MS and Zr/Al series indicate a ~130 kyr period for the short eccentricity and ~ 28 – ~37 kyr cyclicity of the obliquity (Fig. 7). According to astronomical solutions, the amplitude envelope of short-term eccentricity cycle is modulated by long-period eccentricity cycles (Laskar et al., 2004). For example, the precession-

related cycle amplitude envelope is modulated by both the ~100-kyr short eccentricity and 405-kyr long eccentricity. These Myr-scale long-term amplitude modulations of the observed short eccentricity (~130 kyr) and obliquity cycles (~28 – ~37 kyr) are evaluated using the Hilbert Transform of the bandpass-filtered short eccentricity and obliquity signals (e.g., Da Silva et al., 2016; Taner et al., 1979).

Power spectra of eccentricity and obliquity amplitudes in the MS series show significant peaks at ~1.39 Myr and ~ 1.0 Myr and ~ 0.5 Myr, respectively (Fig. 10C and D). Power spectra of eccentricity and obliquity amplitudes in the Zr/Al series reveal peaks at ~1.8 Myr, ~1.2 Myr, and ~ 0.8 Myr as well as ~1.1 Myr, ~0.9 Myr and 0.5 Myr,
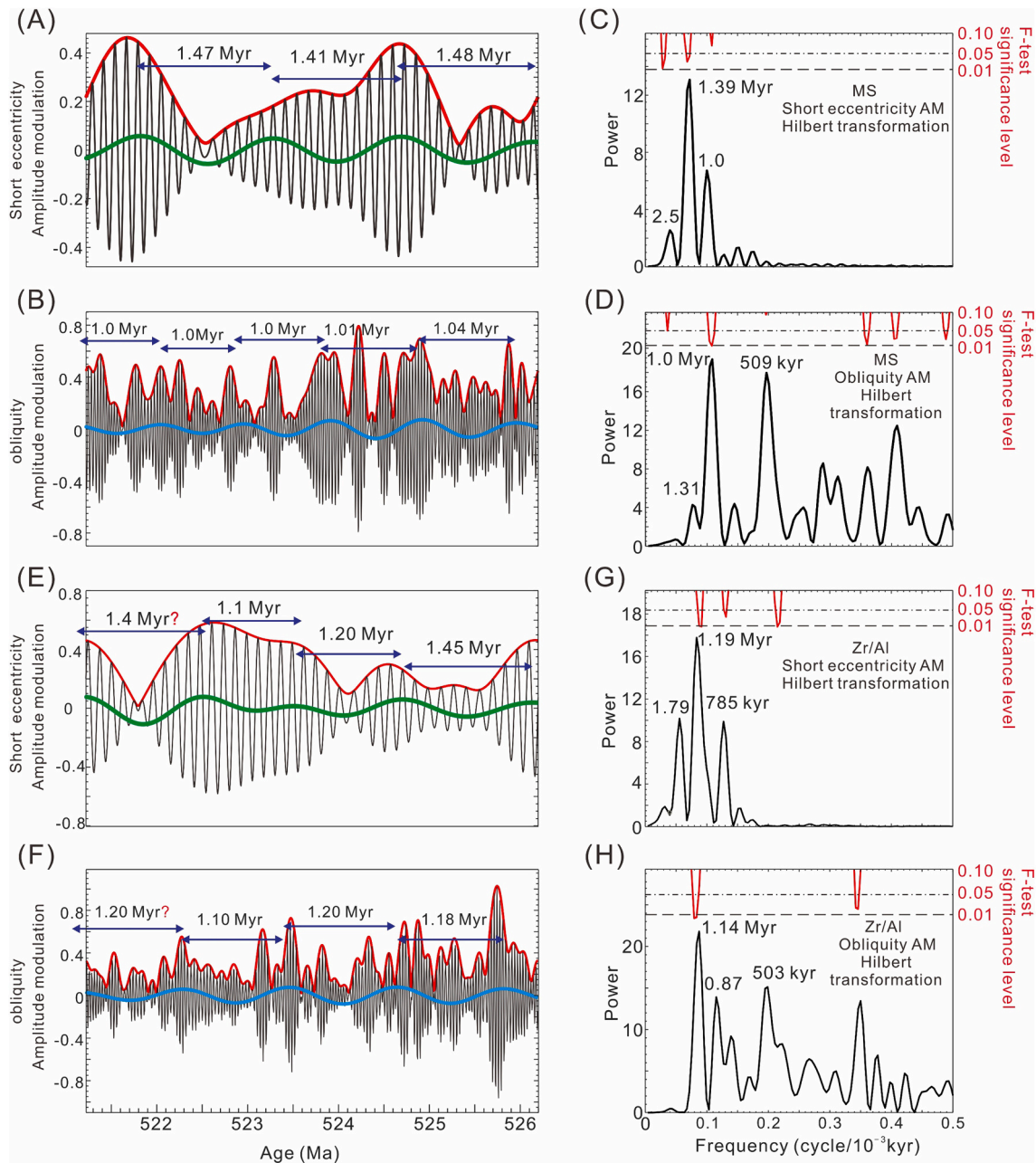

Fig. 10. Amplitude modulation of observed obliquity (~28–37 kyr) and short eccentricity cycles (~130 kyr) of MS and Zr/Al series and their power spectra. (A, B, E and F) Amplitude modulation (AM) envelop curves (red line) were determined by the Hilbert Transform of short eccentricity cycles (bandpass: 0.00785 ± 0.00075 cycles/kyr for MS series and 0.0077 ± 0.0007 cycles/kyr for Zr/Al series, respectively) and obliquity cycles (both bandpass: 0.0031 ± 0.0005 cycles/kyr) from time-calibrated MS and Zr/Al series. Filtered ~1.1 – ~1.5 Myr cycles (green line in panels A and E; bandpass: 0.000675 ± 0.00225 cycles/kyr for MS series and 0.00065 ± 0.00025 cycles/kyr for Zr/Al series, respectively) and ~ 1.0 – ~1.2 Myr cycles (blue line in panel B and F; both bandpass: 0.001 ± 0.0002 cycles/kyr) from amplitude modulations envelop curves of the short eccentricity and obliquity cycles using the bandpass filter. Periodograms of A, B, E and F are shown in C, D, G and H, respectively. (For interpretation of the references to colour in this figure legend, the reader is referred to the web version of this article.)

respectively (Fig. 10G and H). Filtered long-term amplitude modulation cycles from the MS and Zr/Al series exhibit ~1.5 – ~1.1 Myr periods in the orbital eccentricity (Fig. 10A and E) and ~ 1.2 – ~1.0 Myr modulation in the obliquity (Fig. 10 B and F), which could potentially be associated with the present-day ~2.4 Myr eccentricity cycle (i.e., g_4-g_3 term) and ~ 1.2 Myr (i.e., s_4-s_3 term) amplitude modulation cycle of obliquity (Laskar et al., 2011a). Therefore, the Dongxihe record may provide geological evidence for the chaotic motion between Earth and Mars in the Early Cambrian, similar as suggested for the Cretaceous by Ma et al. (2017).

Zhang et al. (2022) reported main periodicities of ~1.2 – ~1.8 Myr (i.e., g_4-g_3 term) and ~ 1.0 – ~1.7 Myr (i.e., s_4-s_3 term) cycles for the long period amplitude modulation of eccentricity and obliquity cycles in gamma-ray logs of the Early Cambrian Qiongzhusi Formation. We note that the g_4-g_3 and s_4-s_3 terms extracted from the three proxies (gamma-ray logs, magnetic susceptibility and Zr/Al) from the Qiongzhusi Formation at Well A (Zhang et al., 2022) and Dongxihe (this study) exhibit different multi-Myr-scale periodicities. Accordingly, multi-Myr amplitude modulation of eccentricity and obliquity cycles in sedimentary records should be assessed appropriately due to the internal non-linear response processes, such as local sedimentary conditions, susceptibility of paleoclimate proxies, as well as other forcings, such as tectonic and volcanic processes (e.g., Ikeda and Tada, 2020). Besides, our dataset spanning ~5 Myr is relatively short for long-term amplitude modulation investigations of short eccentricity cycles. This may be one of the reasons for the discrepancy between the g_4-g_3 term in the Dongxihe record and those reported by Zhang et al. (2022).

Therefore, further investigation of multiple independent studies for the same periods may help to verify these grand cycles observed in the geological records. We compiled multi-Myr cycles of s_4-s_3 and g_4-g_3 terms throughout the Phanerozoic (Fig. 11). Our compilation suggests that the g_4-g_3 term is mainly characterized by ~2.0-Myr cycles to ~2.4-Myr cycles and the s_4-s_3 term presents ~1.0-Myr cycles to ~1.2-Myr cycles in most of the Phanerozoic (Fig. 11). Thus, the secular resonance between the orbits of Earth and Mars is manifested by the present (g_4-g_3)- 2(s_4-s_3) =0 in libration state for most of the Phanerozoic, while the new resonance (g_4-g_3)- (s_4-s_3) = 0 occurs only in a few sporadic short-term intervals (Fig. 11). Collectively, these grand cycles in the Early Cambrian geological records confirm the Solar System behaving chaotically and could be served as constraints for the evolution of the Solar System in deep time.

6. Conclusions

Through our study of orbitally paced tropical climate dynamics of South China in the Early Cambrian (Qiongzhusi Formation), we can propose these four key findings:

(1) The astrochronology of the Qiongzhusi Formation indicates a duration of 4.99 Myr for the studied interval that extends from 526.2 ± 1.91 Ma to 521.23 ± 1.91 Ma. The base age of the Middle Member is constrained at 524.16 ± 1.91 Ma.

(2) The observed quasi-periodic fluctuations in the MS and Zr/Al series of the Qiongzhusi Formation were closely intertwined with monsoon intensity variations and trade wind patterns under the ITCZ-related paleo-Hadley cell dynamics induced by orbital-forced insolation variations. We propose an ITCZ migration model to interpret the relationship between orbitally forced
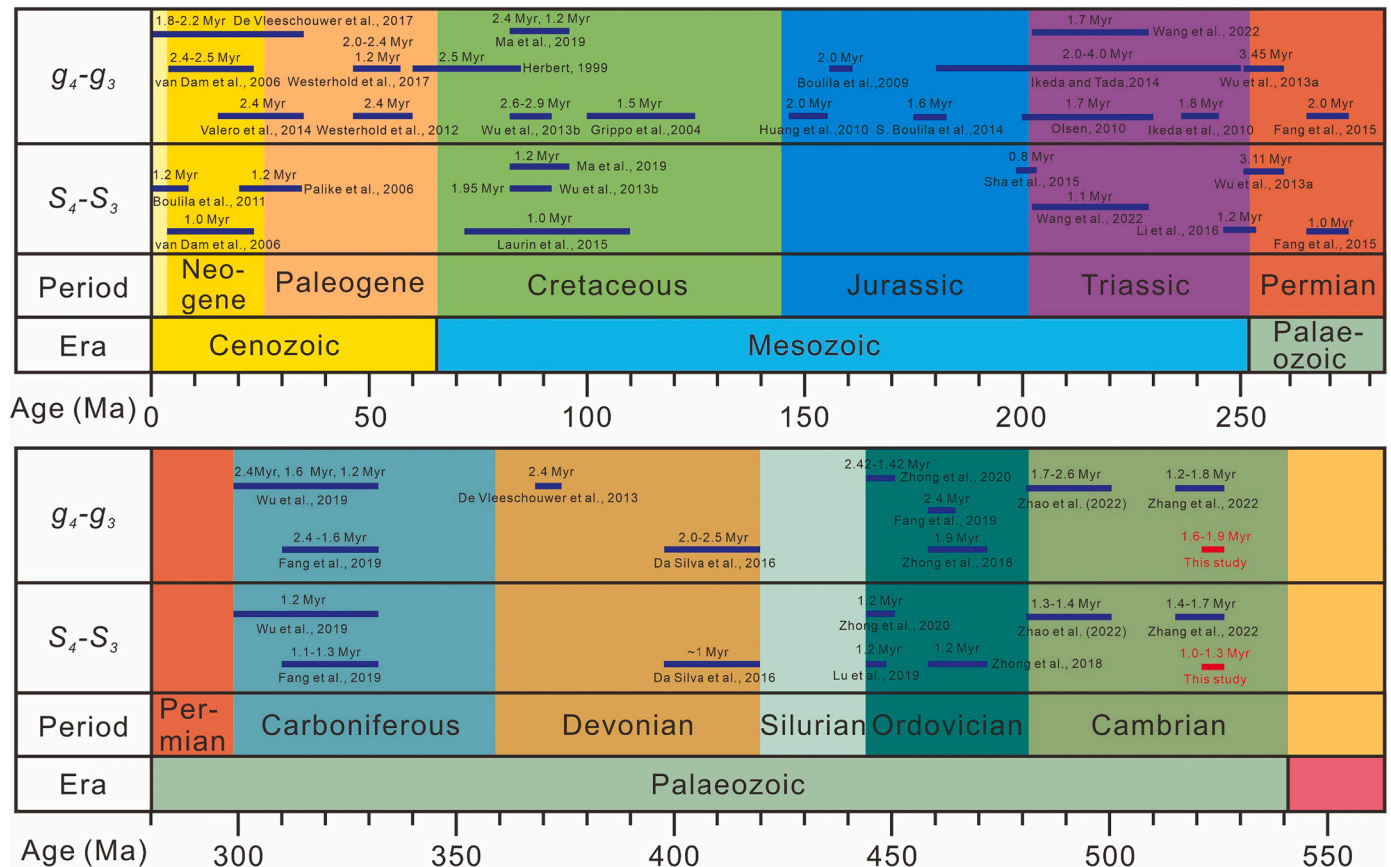

Fig. 11. Compilation of s_4-s_3 term and g_4-g_3 term extracted from the geological records throughout the Phanerozoic Eon (modified from Ma et al. (2019)). References are shown in the figure: Boulila et al., 2010, 2014; Da Silva et al., 2016; De Vleeschouwer et al., 2013; Fang et al., 2015, 2019; Grippo et al., 2004; Herbert, 1999; Huang et al., 2010; Ikeda et al., 2010; Ikeda and Tada, 2020, 2014; Lu et al., 2019; Ma et al., 2019; Olsen, 2010; Sha et al., 2015; Valero et al., 2014; Van Dam et al., 2006; Wang et al., 2022; Westerhold et al., 2012, 2017; Wu et al., 2019, 2013a, 2013b; Zhang et al., 2022; Zhao et al., 2022; Zhong et al., 2020, 2018.

insolation changes, ITCZ migration dynamics, and low-latitude climate processes, consistent with a ~ 5 Myr long dataset of MS and Zr/Al. Specifically, the precession and obliquity forcing shift the mean position of the ITCZ northward/southward by changing the interhemispheric pressure contrasts, thus leading to changes in the low-latitude hydrologic cycle. The intensified obliquity signal within the interval of ~524.8 – ~522.6 Ma is likely associated with cross-equatorial pressure/thermal gradient variations resulting from the episodic development of the Antarctic ice sheet under an Early Cambrian greenhouse lacking permanent ice sheets.

(3) Sub-Milankovitch cycles of ~12.0 – ~6.1 kyr in the Early Cambrian tropic climate archive are identified and 7.9–8.3 kyr cycles are interpreted as corresponding to the semi-precession period, associated with the twice-annual passage of the ITCZ across the intertropical zone.

(4) The ~1.2–1.5 Myr and ~ 1.0–1.2 Myr periods in the amplitude modulation of short eccentricity and obliquity cycles in the MS and Zr/Al series may provide geological evidence for the chaotic motion between Earth and Mars in the Early Cambrian.

CRediT authorship contribution statement

Tan Zhang: Conceptualization, Methodology, Writing – original draft. **Yifan Li:** Writing – review & editing. **Tailiang Fan:** Writing – review & editing. **Anne-Christine Da Silva:** Conceptualization, Methodology, Writing – review & editing. **Mingzhi Kuang:** Data curation, Investigation. **Wangwei Liu:** Data curation, Investigation. **Chao Ma:** Writing – review & editing. **Qi Gao:** Data curation, Investigation. **Juye Shi:** Writing – review & editing. **Zhiqian Gao:** Writing – review & editing. **Mingsong Li:** Conceptualization, Methodology, Writing – review & editing.

Declaration of Competing Interest

The authors declare that they have no known competing financial interests or personal relationships that could have appeared to influence the work reported in this paper.

Data availability

Data are included in Supplementary material 2. Supplementary data to this article can be found online at https://doi.org/10.1016/j.gloplacha.2022.103985.

Acknowledgments

Appendix A. Supplementary data

Supplementary data to this article can be found online at https://doi.org/10.1016/j.gloplacha.2022.103985.

References

Abels, H.A., Aziz, H.A., Krijgsman, W., Smeets, S.J.B., Hilgen, F.J., 2010. Long-period eccentricity control on sedimentary sequences in the continental Madrid Basin (middle Miocene, Spain). Earth Planet. Sci. Lett. 289, 220–231. https://doi.org/10.1016/j.epsl.2009.11.011.

Abels, H.A., Kraus, M.J., Gingerich, P.D., 2013. Precession-scale cyclicity in the fluvial lower Eocene Willwood Formation of the Bighorn Basin, Wyoming (USA). Sedimentology 60, 1467–1483. https://doi.org/10.1111/sed.12039.

Anderson, R.Y., 2011. Enhanced climate variability in the tropics: a 200 000 yr annual record of monsoon variability from Pangea's equator. Clim. Past 7, 757–770. https://doi.org/10.5194/cp-7-757-2011.

Ao, H., Dupont-Nivet, G., Rohling, E.J., Zhang, P., Ladant, J.B., Roberts, A.P., Licht, A., Liu, Q., Liu, Z., Dekkers, M.J., Coxall, H.K., Jin, Z., Huang, C., Xiao, G., Poulsen, C.J., Barbolini, N., Meijer, N., Sun, Q., Qiang, X., Yao, J., An, Z., 2020. Orbital climate variability on the northeastern Tibetan Plateau across the Eocene–Oligocene transition. Nat. Commun. 11, 5249. https://doi.org/10.1038/s41467-020-18824-8.

Armstrong, H.A., Wagner, T., Herringshaw, L.G., Farnsworth, A., Lunt, D.J., Harland, M., Imber, J., Loptson, C., Atar, E.F.L., 2016. Hadley circulation and precipitation changes controling black shale deposition in the late Jurassic Boreal Seaway. Paleoceanography 31, 1041–1053. https://doi.org/10.1002/2015PA002911.

Ashkenazy, Y., Gildor, H., 2008. Timing and significance of maximum and minimum equatorial insolation. Paleoceanography 23. https://doi.org/10.1029/2007PA001436.

Beckmann, B., Flögel, S., Hofmann, P., Schulz, M., Wagner, T., 2005. Orbital forcing of cretaceous river discharge in tropical Africa and ocean response. Nature 437, 241–244. https://doi.org/10.1038/nature03976.

Berger, A., Loutre, M.F., 2009. Astronomical Forcing through Geological Time. In: International Association of Sedimentologists Series. Blackwell Scientific Publications Oxford, pp. 15–24. https://doi.org/10.1002/9781444304039.ch2.

Berger, A., Loutre, M.F., Laskar, J., 1992. Stability of the astronomical frequencies over the earth's history for paleoclimate studies. Science (80-.) 255, 560–566. https://doi.org/10.1126/science.255.5044.560.

Berger, A., Loutre, M.F., Mélice, J.L., 2006. Equatorial insolation: from precession harmonics to eccentricity frequencies. Clim. Past 2, 131–136. https://doi.org/10.5194/cp-2-131-2006.

Bloemendal, J., DeMenocal, P., 1989. Evidence for a change in the periodicity of tropical climate cycles at 2.4 Myr from whole-core magnetic susceptibility measurements. Nature 342, 897–900. https://doi.org/10.1038/342897a0.

Bosmans, J.H.C., Hilgen, F.J., Tuenter, E., Lourens, L.J., 2015. Obliquity forcing of low-latitude climate. Clim. Past 11, 1335–1346. https://doi.org/10.5194/cp-11-1335-2015.

Boulila, S., Galbrun, B., Hinnov, L.A., Collin, P.Y., Ogg, J.G., Fortwengler, D., Marchand, D., 2010. Milankovitch and sub-Milankovitch forcing of the Oxfordian (late Jurassic) Terres Noires Formation (SE France) and global implications. Basin Res. 22, 717–732. https://doi.org/10.1111/j.1365-2117.2009.00429.x.

Boulila, S., Galbrun, B., Huret, E., Hinnov, L.A., Rouget, I., Gardin, S., Bartolini, A., 2014. Astronomical calibration of the Toarcian Stage: Implications for sequence stratigraphy and duration of the early Toarcian OAE. Earth Planet. Sci. Lett. 386, 98–111. https://doi.org/10.1016/j.epsl.2013.10.047.

Brasier, M.D., Magaritz, M., Corfield, R., Huilin, L., Xiche, W., Lin, O., Zhiwen, J., Hamdi, B., Tinggui, H., Fraser, A.G., 1990. The carbon- and oxygen-isotope record of the Precambrian-Cambrian boundary interval in China and Iran and their correlation. Geol. Mag. https://doi.org/10.1017/S0016756800014886.

Broccoli, A.J., Dahl, K.A., Stouffer, R.J., 2006. Response of the ITCZ to Northern Hemisphere cooling. Geophys. Res. Lett. 33, n/a-n/a. https://doi.org/10.1029/2005GL024546.

Cai, W., Lengaigne, M., Borlace, S., Collins, M., Cowan, T., McPhaden, M.J., Timmermann, A., Power, S., Brown, J., Menkes, C., Ngari, A., Vincent, E.M., Widlansky, M.J., 2012. More extreme swings of the South Pacific convergence zone due to greenhouse warming. Nature 488, 365–369. https://doi.org/10.1038/nature11358.

Calvert, S.E., Pedersen, T.F., 2007. Chapter Fourteen Elemental Proxies for Palaeoclimatic and Palaeoceanographic Variability in Marine Sediments: Interpretation and Application. In: Developments in Marine Geology. Elsevier, pp. 567–644. https://doi.org/10.1016/S1572-5480(07)01019-6.

Chiang, J.C.H., 2009. The tropics in paleoclimate. Annu. Rev. Earth Planet. Sci. 37, 263–297. https://doi.org/10.1146/annurev.earth.031208.100217.

Chiang, J.C.H., Friedman, A.R., 2012. Extratropical cooling, interhemispheric thermal gradients, and tropical climate change. Annu. Rev. Earth Planet. Sci. 40, 383–412. https://doi.org/10.1146/annurev-earth-042711-105545.

Chu, R., Wu, H., Zhu, R., Fang, Q., Deng, S., Cui, J., Yang, T., Li, H., Cao, L., Zhang, S., 2020. Orbital forcing of Triassic megamonsoon activity documented in lacustrine sediments from Ordos Basin, China. Palaeogeogr. Palaeoclimatol. Palaeoecol. 541, 109542 https://doi.org/10.1016/j.palaeo.2019.109542.

Clemens, S.C., Tiedemann, R., 1997. Eccentricity forcing of pliocene-early pleistocene climate revealed in a marine oxygen-isotope record. Nature 385, 801–804. https://doi.org/10.1038/385801a0.

Clement, A.C., Hall, A., Broccoli, A.J., 2004. The importance of precessional signals in the tropical climate. Clim. Dyn. 22, 327–341. https://doi.org/10.1007/s00382-003-0375-8.

Cleveland, W.S., 1979. Robust locally weighted regression and smoothing scatterplots. J. Am. Stat. Assoc. 74, 829–836. https://doi.org/10.1080/01621459.1979.10481038.

Compston, W., Zhang, Z., Cooper, J.A., Ma, G., Jenkins, R.J.F., 2008. Further shrimp geochronology on the early Cambrian of South China. Am. J. Sci. 308, 399–420. https://doi.org/10.2475/04.2008.01.

Cramer, B.S., Wright, J.D., Kent, D.V., Aubry, M.P., 2003. Orbital climate forcing of δ13C excursions in the late Paleocene-early Eocene (chrons C24n-C25n). Paleoceanography 18, n/a–n/a. https://doi.org/10.1029/2003PA000909.

Crowley, T.J., Kim, K.Y., Mengel, J.G., Short, D.A., 1992. Modeling 100,000-year climate fluctuations in pre-pleistocene time series. Science 80-.). 255, 705–707. https://doi.org/10.1126/science.255.5045.705.

Da Silva, A.C., De Vleeschouwer, D., Boulvain, F., Claeys, P., Fagel, N., Humblet, M., Mabille, C., Michel, J., Sardar Abadi, M., Pas, D., Dekkers, M.J., 2013. Magnetic susceptibility as a high-resolution correlation tool and as a climatic proxy in Paleozoic rocks - Merits and pitfalls: examples from the Devonian in Belgium. Mar. Pet. Geol. 46, 173–189. https://doi.org/10.1016/j.marpetgeo.2013.06.012.

Da Silva, A.C., Hladil, J., Chadimová, L., Slavík, L., Hilgen, F.J., Bábek, O., Dekkers, M.J., 2016. Refining the Early Devonian time scale using Milankovitch cyclicity in Lochkovian–Pragian sediments (Prague Synform, Czech Republic). Earth Planet. Sci. Lett. 455, 125–139. https://doi.org/10.1016/j.epsl.2016.09.009.

Da Silva, A.C., Dekkers, M.J., De Vleeschouwer, D., Hladil, J., Chadimova, L., Slavík, L., Hilgen, F.J., 2019. Millennial-scale climate changes manifest Milankovitch combination tones and Hallstatt solar cycles in the Devonian greenhouse world. Geology 47, e489–e490. https://doi.org/10.1130/G46732Y.1.

Da Silva, A.C., Sinnesael, M., Claeys, P., Davies, J.H.F.L., de Winter, N.J., Percival, L.M. E., Schaltegger, U., De Vleeschouwer, D., 2020. Anchoring the late Devonian mass extinction in absolute time by integrating climatic controls and radio-isotopic dating. Sci. Rep. 10, 12940. https://doi.org/10.1038/s41598-020-69097-6.

De Vleeschouwer, D., Da Silva, A.C., Boulvain, F., Crucifix, M., Claeys, P., 2012. Precessional and half-precessional climate forcing of Mid-Devonian monsoon-like dynamics. Clim. Past 8, 337–351. https://doi.org/10.5194/cp-8-337-2012.

De Vleeschouwer, D., Rakociński, M., Racki, G., Bond, D.P.G., Sobień, K., Claeys, P., 2013. The astronomical rhythm of Late-Devonian climate change (Kowala section, Holy Cross Mountains, Poland). Earth Planet. Sci. Lett. 365, 25–37. https://doi.org/10.1016/j.epsl.2013.01.016.

Dong, Y., Zhang, G., Neubauer, F., Liu, X., Genser, J., Hauzenberger, C., 2011. Tectonic evolution of the Qinling orogen, China: Review and synthesis. J. Asian Earth Sci. 41, 213–237. https://doi.org/10.1016/j.jseaes.2011.03.002.

Ellwood, B.B., Wang, W.H., Tomkin, J.H., Ratcliffe, K.T., El Hassani, A., Wright, A.M., 2013. Testing high resolution magnetic susceptibility and gamma radiation methods in the Cenomanian-Turonian (Upper cretaceous) GSSP and near-by coeval section. Palaeogeogr. Palaeoclimatol. Palaeoecol. 378, 75–90. https://doi.org/10.1016/j.palaeo.2013.02.018.

Elrick, M., Hinnov, L.A., 2007. Millennial-scale paleoclimate cycles recorded in widespread Palaeozoic deeper water rhythmites of North America. Palaeogeogr. Palaeoclimatol. Palaeoecol. 243, 348–372. https://doi.org/10.1016/j.palaeo.2006.08.008.

Fang, Q., Wu, H., Hinnov, L.A., Jing, X., Wang, X., Jiang, Q., 2015. Geologic evidence for chaotic behavior of the planets and its constraints on the third-order eustatic sequences at the end of the late Paleozoic Ice Age. Palaeogeogr. Palaeoclimatol. Palaeoecol. 440, 848–859. https://doi.org/10.1016/j.palaeo.2015.10.014.

Fang, J., Wu, H., Fang, Q., Shi, M., Zhang, S., Yang, T., Li, H., Cao, L., 2020. Cyclostratigraphy of the global stratotype section and point (GSSP) of the basal Guzhangian Stage of the Cambrian Period. Palaeogeogr. Palaeoclimatol. Palaeoecol. 540, 109530 https://doi.org/10.1016/j.palaeo.2019.109530.

Fang, Q., Wu, H., Wang, X., Yang, T., Li, H., Zhang, S., 2019. An astronomically forced cooling event during the Middle Ordovician. Glob. Planet. Change 173, 96–108. https://doi.org/10.1016/j.gloplacha.2018.12.010.

Ferretti, P., Crowhurst, S.J., Naafs, B.D.A., Barbante, C., 2015. The Marine Isotope Stage 19 in the mid-latitude North Atlantic Ocean: Astronomical signature and intra-interglacial variability. Quat. Sci. Rev. 108, 95–110. https://doi.org/10.1016/j.quascirev.2014.10.024.

Fitzpatrick, R.W., Chittleborough, D.J., 2018. Titanium and zirconium minerals. Soil Mineral. with Environ. Appl. 7, 667–690. https://doi.org/10.2136/sssabookser7.c22.

Fox, B.R.S., D'Andrea, W.J., Wilson, G.S., Lee, D.E., Wartho, J.A., 2017. Interaction of polar and tropical influences in the mid-latitudes of the Southern Hemisphere during the Mi-1 deglaciation. Glob. Planet. Change 155, 109–120. https://doi.org/10.1016/j.gloplacha.2017.06.008.

Gadgil, S., 2003. The Indian monsoon and its variability. Annu. Rev. Earth Planet. Sci. 31, 429–467. https://doi.org/10.1146/annurev.earth.31.100901.141251.

Grippo, A., Fischer, A.G., Hinnov, L.A., Herbert, T.D., Silva, I.P., 2004. Cyclostratigraphy and chronology of the albian stage (piobbico core, Italy). In: Cyclostratigraphy: Approaches and Case Histories. SEPM, Society for Sedimentary Geology, pp. 57–81. https://doi.org/10.2110/pec.04.81.0057.

Haug, G.H., Hughen, K.A., Sigman, D.M., Peterson, L.C., Röhl, U., 2001. Southward migration of the intertropical convergence zone through the holocene. Science 80-.). 293, 1304–1308. https://doi.org/10.1126/science.1059725.

Hearing, T.W., Harvey, T.H.P., Williams, M., Leng, M.J., Lamb, A.L., Wilby, P.R., Gabbott, S.E., Pohl, A., Donnadieu, Y., 2018. An early Cambrian greenhouse climate. Sci. Adv. 4, eaar5690. https://doi.org/10.1126/sciadv.aar5690.

Heitmann, E.O., Ji, S., Nie, J., Breecker, D.O., 2017. Orbitally-paced variations of water availability in the SE Asian Monsoon region following the Miocene climate transition. Earth Planet. Sci. Lett. 474, 272–282. https://doi.org/10.1016/j.epsl.2017.06.006.

Herbert, T.D., 1999. Toward a composite orbital chronology for the late cretaceous and early Palaeocene GPTS. Philos. Trans. R. Soc. A Math. Phys. Eng. Sci. 357, 1891–1905. https://doi.org/10.1098/rsta.1999.0406.

Hinnov, L.A., 2000. New perspectives on orbitally forced stratigraphy. Annu. Rev. Earth Planet. Sci. 28, 419–475. https://doi.org/10.1146/annurev.earth.28.1.419.

Hinnov, L.A., 2013. Cyclostratigraphy and its revolutionizing applications in the earth and planetary sciences. Bull. Geol. Soc. Am. 125, 1703–1734. https://doi.org/10.1130/B30934.1.

Hofmann, P., Wagner, T., 2011. ITCZ controls on late cretaceous black shale sedimentation in the tropical Atlantic Ocean. Paleoceanography 26. https://doi.org/10.1029/2011PA002154.

Huang, C., Hesselbo, S.P., Hinnov, L., 2010. Astrochronology of the late Jurassic Kimmeridge Clay (Dorset, England) and implications for Earth system processes. Earth Planet. Sci. Lett. 289, 242–255. https://doi.org/10.1016/j.epsl.2009.11.013.

Huang, E., Wang, P., Wang, Y., Yan, M., Tian, J., Li, S., Ma, W., 2020. Dole effect as a measurement of the low-latitude hydrological cycle over the past 800 ka. Sci. Adv. 6, eaba4823. https://doi.org/10.1126/sciadv.aba4823.

Ikeda, M., Tada, R., 2014. A 70 million year astronomical time scale for the deep-sea bedded chert sequence (Inuyama, Japan): Implications for Triassic-Jurassic geochronology. Earth Planet. Sci. Lett. 399, 30–43. https://doi.org/10.1016/j.epsl.2014.04.031.

Ikeda, M., Tada, R., 2020. Reconstruction of the chaotic behavior of the Solar System from geologic records. Earth Planet. Sci. Lett. 537, 116168 https://doi.org/10.1016/j.epsl.2020.116168.

Ikeda, M., Tada, R., Sakuma, H., 2010. Astronomical cycle origin of bedded chert: a middle Triassic bedded chert sequence, Inuyama, Japan. Earth Planet. Sci. Lett. 297, 369–378. https://doi.org/10.1016/j.epsl.2010.06.027.

Jian, Z., Wang, Y., Dang, H., Lea, D.W., Liu, Z., Jin, H., Yin, Y., 2020. Half-precessional cycle of thermocline temperature in the western equatorial Pacific and its bihemispheric dynamics. Proc. Natl. Acad. Sci. U. S. A. 117, 7044–7051. https://doi.org/10.1073/pnas.1915510117.

Jiang, G., Wang, X., Shi, X., Xiao, S., Zhang, S., Dong, J., 2012. The origin of decoupled carbonate and organic carbon isotope signatures in the early Cambrian (ca. 542-520Ma) Yangtze platform. Earth Planet. Sci. Lett. 317–318, 96–110. https://doi.org/10.1016/j.epsl.2011.11.018.

Jin, Z., Cao, J., Wu, J., Wang, S., 2006. A Rb/Sr record of catchment weathering response to Holocene climate change in Inner Mongolia. Earth Surf. Process. Landforms 31, 285–291. https://doi.org/10.1002/esp.1243.

Jin, C., Li, C., Algeo, T.J., Planavsky, N.J., Cui, H., Yang, X., Zhao, Y., Zhang, X., Xie, S., 2016. A highly redox-heterogeneous ocean in South China during the early Cambrian (~529-514 Ma): Implications for biota-environment co-evolution. Earth Planet. Sci. Lett. 441, 38–51. https://doi.org/10.1016/j.epsl.2016.02.019.

Jin, Z., Yu, J., Zhang, F., Qiang, X., 2020. Glacial-interglacial variation in catchment weathering and erosion paces the Indian summer monsoon during the Pleistocene. Quat. Sci. Rev. 248, 106619 https://doi.org/10.1016/j.quascirev.2020.106619.

Kodama, K.P., Hinnov, L.A., 2014. Rock Magnetic Cyclostratigraphy. John Wiley & Sons, Rock Magnetic Cyclostratigraphy. https://doi.org/10.1002/9781118561294.

Koutavas, A., deMenocal, P.B., Olive, G.C., Lynch-Stieglitz, J., 2006. Mid-Holocene El Niño-Southern Oscillation (ENSO) attenuation revealed by individual foraminifera in eastern tropical Pacific sediments. Geology 34, 993–996. https://doi.org/10.1130/G22810A.1.

Laskar, J., 1989. A numerical experiment on the chaotic behaviour of the Solar System. Nature 338, 237–238. https://doi.org/10.1038/338237a0.

Laskar, J., 1990. The chaotic motion of the solar system: a numerical estimate of the size of the chaotic zones. Icarus 88, 266–291. https://doi.org/10.1016/0019-1035(90)90084-M.

Laskar, J., Robutel, P., Joutel, F., Gastineau, M., Correia, A.C.M., Levrard, B., 2004. A long-term numerical solution for the insolation quantities of the Earth. Astron. Astrophys. 428, 261–285. https://doi.org/10.1051/0004-6361:20041335.

Laskar, J., Fienga, A., Gastineau, M., Manche, H., 2011a. La2010: a new orbital solution for the long-term motion of the Earth. Astron. Astrophys. 532, A89. https://doi.org/10.1051/0004-6361/201116836.

Laskar, J., Gastineau, M., Delisle, J.B., Farrés, A., Fienga, A., 2011b. Strong chaos induced by close encounters with Ceres and Vesta. Astron. Astrophys. 532, L4. https://doi.org/10.1051/0004-6361/201117504.

Lear, C.H., Bailey, T.R., Pearson, P.N., Coxall, H.K., Rosenthal, Y., 2008. Cooling and ice growth across the Eocene-Oligocene transition. Geology 36, 251–254. https://doi.org/10.1130/G24584A.1.

Levy, R.H., Meyers, S.R., Naish, T.R., Golledge, N.R., McKay, R.M., Crampton, J.S., DeConto, R.M., De Santis, L., Florindo, F., Gasson, E.G.W., Harwood, D.M., Luyendyk, B.P., Powell, R.D., Clowes, C., Kulhanek, D.K., 2019. Antarctic ice-sheet sensitivity to obliquity forcing enhanced through ocean connections. Nat. Geosci. 12, 132–137. https://doi.org/10.1038/s41561-018-0284-4.

Li, Z.X., Bogdanova, S.V., Collins, A.S., Davidson, A., De Waele, B., Ernst, R.E., Fitzsimons, I.C.W., Fuck, R.A., Gladkochub, D.P., Jacobs, J., Karlstrom, K.E., Lu, S., Natapov, L.M., Pease, V., Pisarevsky, S.A., Thrane, K., Vernikovsky, V., 2008. Assembly, configuration, and break-up history of Rodinia: a synthesis. Precambrian Res. 160, 179–210. https://doi.org/10.1016/j.precamres.2007.04.021.

Li, M., Huang, C., Hinnov, L., Ogg, J., Chen, Z.Q., Zhang, Y., 2016. Obliquity-forced climate during the early Triassic hothouse in China. Geology 44, 623–626. https://doi.org/10.1130/G37970.1.

Li, M., Kump, L.R., Hinnov, L.A., Mann, M.E., 2018. Tracking variable sedimentation rates and astronomical forcing in Phanerozoic paleoclimate proxy series with evolutionary correlation coefficients and hypothesis testing. Earth Planet. Sci. Lett. 501, 165–179. https://doi.org/10.1016/j.epsl.2018.08.041.

Li, M., Hinnov, L., Kump, L., 2019a. Acycle: Time-series analysis software for paleoclimate research and education. Comput. Geosci. 127, 12–22. https://doi.org/10.1016/j.cageo.2019.02.011.

Li, M., Huang, C., Ogg, J., Zhang, Y., Hinnov, L., Wu, H., Chen, Z.Q., Zou, Z., 2019b. Paleoclimate proxies for cyclostratigraphy: Comparative analysis using a lower

Triassic marine section in South China. Earth-Science Rev. 189, 125–146. https://doi.org/10.1016/j.earscirev.2019.01.011.

Liu, Y., Lo, L., Shi, Z., Wei, K.Y., Chou, C.J., Chen, Y.C., Chuang, C.K., Wu, C.C., Mii, H.S., Peng, Z., Amakawa, H., Burr, G.S., Lee, S.Y., Delong, K.L., Elderfield, H., Shen, C.C., 2015. Obliquity pacing of the western Pacific Intertropical Convergence Zone over the past 282,000 years. Nat. Commun. 6 https://doi.org/10.1038/ncomms10018.

Liu, D., Huang, C., Kemp, D.B., Li, M., Ogg, J.G., Yu, M., Foster, W.J., 2021. Paleoclimate and sea level response to orbital forcing in the Middle Triassic of the eastern Tethys. Glob. Planet. Change 199, 103454. https://doi.org/10.1016/j.gloplacha.2021.103454.

Lu, Yangbo, Huang, C., Jiang, S., Zhang, J., Lu, Yongchao, Liu, Y., 2019. Cyclic late Katian through Hirnantian glacioeustasy and its control of the development of the organic-rich Wufeng and Longmaxi shales, South China. Palaeogeogr. Palaeoclimatol. Palaeoecol. 526, 96–109. https://doi.org/10.1016/j.palaeo.2019.04.012.

Ma, C., Meyers, S.R., Sageman, B.B., 2017. Theory of chaotic orbital variations confirmed by cretaceous geological evidence. Nature 542, 468–470. https://doi.org/10.1038/nature21402.

Ma, C., Meyers, S.R., Sageman, B.B., 2019. Testing late cretaceous astronomical solutions in a 15 million year astrochronologic record from North America. Earth Planet. Sci. Lett. 513, 1–11. https://doi.org/10.1016/j.epsl.2019.01.053.

Mamalakis, A., Randerson, J.T., Yu, J.Y., Pritchard, M.S., Magnusdottir, G., Smyth, P., Levine, P.A., Yu, S., Foufoula-Georgiou, E., 2021. Zonally contrasting shifts of the tropical rain belt in response to climate change. Nat. Clim. Chang. 11, 143–151. https://doi.org/10.1038/s41558-020-00963-x.

Mann, M.E., Lees, J.M., 1996. Robust estimation of background noise and signal detection in climatic time series. Clim. Chang. 33, 409–445. https://doi.org/10.1007/BF00142586.

Martinez, M., Kotov, S., De Vleeschouwer, D., Pas, D., Pälike, H., 2016. Testing the impact of stratigraphic uncertainty on spectral analyses of sedimentary series. Clim. Past 12, 1765–1783. https://doi.org/10.5194/cp-12-1765-2016.

Mayewski, P.A., Meeker, L.D., Twickler, M.S., Whitlow, S., Yang, Q., Lyons, W.B., Prentice, M., 1997. Major features and forcing of high-latitude northern hemisphere atmospheric circulation using a 110,000-year-long glaciochemical series. J. Geophys. Res. Ocean. 102, 26345–26366. https://doi.org/10.1029/96JC03365.

Milankovitch, M., 1941. Kanon der Erdbestrahlung und seine Anwendung auf das Eiszeitenproblem. Königliche Serbische Akad. 633.

Mou, C., Liang, W., Zhou, K., Ge, X., Kang, J., Chen, X., 2012. Sedimentary facies and palaeogeography of the middle-upper Yangtze area during the early Cambrian (Terreneuvian-Series 2). Sediment. Geol. Tethyan Geol. 32, 41–53.

Olsen, P.E., 2010. Fossil great lakes of the Newark Supergroup - 30 years later. In: Field Trip Guidebook, 83rd Annual Meeting New York State Geological Association. Citeseer, pp. 101–162.

Omar, H., Da Silva, A.C., Yaich, C., 2021. Linking the Variation of Sediment Accumulation Rate to Short Term Sea-Level Change Using Cyclostratigraphy: Case Study of the Lower Berriasian Hemipelagic Sediments in Central Tunisia (Southern Tethys). Front. Earth Sci. 9, 176. https://doi.org/10.3389/feart.2021.638441.

Paillard, D., 2010. Climate and the orbital parameters of the Earth. Comptes Rendus - Geosci. 342, 273–285. https://doi.org/10.1016/j.crte.2009.12.006.

Peterson, L.C., Haug, G.H., Hughen, K.A., Rohl, U., 2000. Rapid changes in the hydrologic cycle of the tropical Atlantic during the last glacial. Science 80-.). 290, 1947–1951. https://doi.org/10.1126/science.290.5498.1947.

Philander, S.G.H., Gu, D., Halpern, D., Lambert, G., Lau, N.C., Li, T., Pacanowski, R.C., 1996. Why the ITCZ is mostly north of the equator. J. Clim. 9, 2958–2972. https://doi.org/10.1175/1520-0442(1996)009<2958:WTIIMN>2.0.CO;2.

Pierrehumbert, R.T., 2000. Climate change and the tropical Pacific: the sleeping dragon wakes. Proc. Natl. Acad. Sci. U. S. A. 97, 1355–1358. https://doi.org/10.1073/pnas.97.4.1355.

Prell, W.L., Kutzbach, J.E., 1992. Sensitivity of the Indian monsoon to forcing parameters and implications for its evolution. Nature 360, 647–652. https://doi.org/10.1038/360647a0.

Rea, D.K., Snoeckx, I., Joseph, L.H., 1998. Late Cenozoic Eolian deposition in the North Pacific: Asian drying, Tibetan uplift, and cooling of the northern hemisphere. Paleoceanography 13, 215–224. https://doi.org/10.1029/98PA00123.

Riquier, L., Averbuch, O., Devleeschouwer, X., Tribovillard, N., 2010. Diagenetic versus detrital origin of the magnetic susceptibility variations in some carbonate Frasnian-Famennian boundary sections from Northern Africa and Western Europe: Implications for paleoenvironmental reconstructions. Int. J. Earth Sci. 99, 57–73. https://doi.org/10.1007/s00531-009-0492-7.

Ruhl, M., Hesselbo, S.P., Hinnov, L., Jenkyns, H.C., Xu, W., Riding, J.B., Storm, M., Minisini, D., Ullmann, C.V., Leng, M.J., 2016. Astronomical constraints on the duration of the early Jurassic Pliensbachian Stage and global climatic fluctuations. Earth Planet. Sci. Lett. 455, 149–165. https://doi.org/10.1016/j.epsl.2016.08.038.

Saker-Clark, M., Kemp, D.B., Coe, A.L., 2019. Portable X-Ray Fluorescence Spectroscopy as a Tool for Cyclostratigraphy. Geochemistry. Geophys. Geosystems 20, 2531–2541. https://doi.org/10.1029/2018GC007582.

Schneider, T., Bischoff, T., Haug, G.H., 2014. Migrations and dynamics of the intertropical convergence zone. Nature 513, 45–53. https://doi.org/10.1038/nature13636.

Sha, J., Olsen, P.E., Pan, Y., Xu, D., Wang, Y., Zhang, X., Yao, X., Vajda, V., 2015. Triassic-Jurassic climate in continental high-latitude Asia was dominated by obliquity-paced variations (Junggar Basin, Ürümqi, China). Proc. Natl. Acad. Sci. U. S. A. 112, 3624–3629. https://doi.org/10.1073/pnas.1501137112.

Short, D.A., Mengel, J.G., Crowley, T.J., Hyde, W.T., North, G.R., 1991. Filtering of milankovitch cycles by earth's geography. Quat. Res. 35, 157–173. https://doi.org/10.1016/0033-5894(91)90064-C.

Sinnesael, M., de Winter, N.J., Snoeck, C., Montanari, A., Claeys, P., 2018. An integrated pelagic carbonate multi-proxy study using portable X-ray fluorescence (pXRF): Maastrichtian strata from the Bottaccione Gorge, Gubbio, Italy. Cretac. Res. 91, 20–32. https://doi.org/10.1016/j.cretres.2018.04.010.

Sinnesael, M., De Vleeschouwer, D., Zeeden, C., Batenburg, S.J., Da Silva, A.C., de Winter, N.J., Dinarès-Turell, J., Drury, A.J., Gambacorta, G., Hilgen, F.J., Hinnov, L.A., Hudson, A.J.L., Kemp, D.B., Lantink, M.L., Laurin, J., Li, M., Liebrand, D., Ma, C., Meyers, S.R., Monkenbusch, J., Montanari, A., Nohl, T., Pälike, H., Pas, D., Ruhl, M., Thibault, N., Vahlenkamp, M., Valero, L., Wouters, S., Wu, H., Claeys, P., 2019. The Cyclostratigraphy Intercomparison Project (CIP): consistency, merits and pitfalls. Earth-Science Rev. 199, 102965 https://doi.org/10.1016/j.earscirev.2019.102965.

Sinnesael, M., McLaughlin, P.I., Desrochers, A., Mauviel, A., De Weirdt, J., Claeys, P., Vandenbroucke, T.R.A., 2021. Precession-driven climate cycles and time scale prior to the Hirnantian glacial maximum. Geology 49, 1295–1300. https://doi.org/10.1130/G49083.1.

Sloan, L.C., Huber, M., 2001. Eocene oceanic responses to orbital forcing on precessional time scales. Paleoceanography 16, 101–111. https://doi.org/10.1029/1999PA000491.

Sørensen, A.L., Nielsen, A.T., Thibault, N., Zhao, Z., Schovsbo, N.H., Dahl, T.W., 2020. Astronomically forced climate change in the late Cambrian. Earth Planet. Sci. Lett. 548, 116475 https://doi.org/10.1016/j.epsl.2020.116475.

Steiner, M., Li, G., Qian, Y., Zhu, M., Erdtmann, B.D., 2007. Neoproterozoic to early Cambrian small shelly fossil assemblages and a revised biostratigraphic correlation of the Yangtze Platform (China). Palaeogeogr. Palaeoclimatol. Palaeoecol. 254, 67–99. https://doi.org/10.1016/j.palaeo.2007.03.046.

Sun, J., Huang, X., 2006. Half-precessional cycles recorded in Chinese loess: response to low-latitude insolation forcing during the last Interglaciation. Quat. Sci. Rev. 25, 1065–1072. https://doi.org/10.1016/j.quascirev.2005.08.004.

Taner, M.T., Koehler, F., Sheriff, R.E., 1979. Complex Seismic Trace Analysis. Geophysics 44, 1041–1063. https://doi.org/10.1190/1.1440994.

Taylor, S.R., McLennan, S.M., 1985. The continental crust: its composition and evolution.

Ulfers, A., Zeeden, C., Voigt, S., Sardar Abadi, M., Wonik, T., 2022. Half-precession signals in Lake Ohrid (Balkan) and their spatio-temporal relations to climate records from the European realm. Quat. Sci. Rev. 280, 107413 https://doi.org/10.1016/j.quascirev.2022.107413.

Valero, L., Garcés, M., Cabrera, L., Costa, E., Sáez, A., 2014. 20 Myr of eccentricity paced lacustrine cycles in the Cenozoic Ebro Basin. Earth Planet. Sci. Lett. 408, 183–193. https://doi.org/10.1016/j.epsl.2014.10.007.

Valero, L., Cabrera, L., Sáez, A., Garcés, M., 2016. Long-period astronomically-forced terrestrial carbon sinks. Earth Planet. Sci. Lett. 444, 131–138. https://doi.org/10.1016/j.epsl.2016.03.038.

Van Dam, J.A., Abdul Aziz, H., Sierra, M.Á.Á., Hilgen, F.J., Van Den Hoek Ostende, L.W., Lourens, L.J., Mein, P., Van Der Meulen, A.J., Pelaez-Campomanes, P., 2006. Long-period astronomical forcing of mammal turnover. Nature 443, 687–691. https://doi.org/10.1038/nature05163.

Verschuren, D., Sinninghe Damsté, J.S., Moernaut, J., Kristen, I., Blaauw, M., Fagot, M., Haug, G.H., 2009. Half-precessional dynamics of monsoon rainfall near the East African Equator. Nature 462, 637–641. https://doi.org/10.1038/nature08520.

Wagner, T., Hofmann, P., Flögel, S., 2013. Marine black shale deposition and Hadley Cell dynamics: a conceptual framework for the cretaceous Atlantic Ocean. Mar. Pet. Geol. 43, 222–238. https://doi.org/10.1016/j.marpetgeo.2013.02.005.

Waliser, D.E., Gautier, C., 1993. A satellite-derived climatology of the ITCZ. J. Clim. 6, 2162–2174. https://doi.org/10.1175/1520-0442(1993)006<2162:ASDCOT>2.0.CO;2.

Waltham, D., 2015. Milankovitch period uncertainties and their impact on cyclostratigraphy. J. Sediment. Res. 85, 990–998. https://doi.org/10.2110/jsr.2015.66.

Wang, P., 2021. Low-latitude forcing: a new insight into paleo-climate changes. Innov. 2, 100145 https://doi.org/10.1016/j.xinn.2021.100145.

Wang, J., Li, Z.X., 2003. History of neoproterozoic rift basins in South China: Implications for Rodinia break-up. Precambrian Res. 122, 141–158. https://doi.org/10.1016/S0301-9268(02)00209-7.

Wang, X., Auler, A.S., Edwards, L.L., Cheng, H., Cristalli, P.S., Smart, P.L., Richards, D.A., Shen, C.C., 2004. Wet periods in northeastern Brazil over the past 210 kyr linked to distant climate anomalies. Nature 432, 740–743. https://doi.org/10.1038/nature03067.

Wang, Y., Cheng, H., Edwards, R.L., Kong, X., Shao, X., Chen, S., Wu, J., Jiang, X., Wang, X., An, Z., 2008. Millennial- and orbital-scale changes in the East Asian monsoon over the past 224,000 years. Nature 451, 1090–1093. https://doi.org/10.1038/nature06692.

Wang, M., Li, M., Kemp, D.B., Boulila, S., Ogg, J.G., 2022. Sedimentary noise modeling of lake-level change in the Late Triassic Newark Basin of North America. Glob. Planet. Change 208, 103706. https://doi.org/10.1016/j.gloplacha.2021.103706.

Wang, P.X., Wang, B., Cheng, H., Fasullo, J., Guo, Z.T., Kiefer, T., Liu, Z.Y., 2014. The global monsoon across timescales: Coherent variability of regional monsoons. Clim. Past 10, 2007–2052. https://doi.org/10.5194/cp-10-2007-2014.

Wang, P.X., Wang, B., Cheng, H., Fasullo, J., Guo, Z.T., Kiefer, T., Liu, Z.Y., 2017. The global monsoon across time scales: Mechanisms and outstanding issues. Earth-Science Rev. 174, 84–121. https://doi.org/10.1016/j.earscirev.2017.07.006.

Wang, Z., Zhang, Z., Huang, C., Shen, J., Sui, Y., Qian, Z., 2021. Astronomical forcing of lake evolution in the Lanzhou Basin during early Miocene period. Earth Planet. Sci. Lett. 554, 116648 https://doi.org/10.1016/j.epsl.2020.116648.

Westerhold, T., Röhl, U., Laskar, J., 2012. Time scale controversy: Accurate orbital calibration of the early Paleogene. Geochemistry. Geophys. Geosystems 13, 1–19. https://doi.org/10.1029/2012GC004096.

Westerhold, T., Röhl, U., Frederichs, T., Agnini, C., Raffi, I., Zachos, J.C., Wilkens, R.H., 2017. Astronomical calibration of the Ypresian timescale: Implications for seafloor spreading rates and the chaotic behavior of the solar system? Clim. Past 13, 1129–1152. https://doi.org/10.5194/cp-13-1129-2017.

Whiteside, J.H., Grogan, D.S., Olsen, P.E., Kent, D.V., 2011. Climatically driven biogeographic provinces of late Triassic tropical Pangea. Proc. Natl. Acad. Sci. U. S. A. 108, 8972–8977. https://doi.org/10.1073/pnas.1102473108.

Williams, G.E., 2000. Geological constraints on the Precambrian history of earth's rotation and the moon's orbit. Rev. Geophys. 38, 37–59. https://doi.org/10.1029/1999RG900016.

Winguth, A., Winguth, C., 2013. Precession-driven monsoon variability at the Permian-Triassic boundary - Implications for anoxia and the mass extinction. Glob. Planet. Change 105, 160–170. https://doi.org/10.1016/j.gloplacha.2012.06.006.

Wotte, T., Skovsted, C.B., Whitehouse, M.J., Kouchinsky, A., 2019. Isotopic evidence for temperate oceans during the Cambrian Explosion. Sci. Rep. 9, 6330. https://doi.org/10.1038/s41598-019-42719-4.

Wu, H., Zhang, S., Hinnov, L.A., Jiang, G., Feng, Q., Li, H., Yang, T., 2013a. Time-calibrated Milankovitch cycles for the late Permian. Nat. Commun. 4, 1–8. https://doi.org/10.1038/ncomms3452.

Wu, H., Zhang, S., Hinnov, L.A., Jiang, G., Feng, Q., Li, H., Yang, T., 2013a. Time-calibrated Milankovitch cycles for the late Permian. Nat. Commun. 4, 1–8. https://doi.org/10.1038/ncomms3452.

Wu, H., Zhang, S., Jiang, G., Hinnov, L., Yang, T., Li, H., Wan, X., Wang, C., 2013b. Astrochronology of the early Turonian-early Campanian terrestrial succession in the Songliao Basin, northeastern China and its implication for long-period behavior of the Solar System. Palaeogeogr. Palaeoclimatol. Palaeoecol. 385, 55–70. https://doi.org/10.1016/j.palaeo.2012.09.004.

Wu, H., Fang, Q., Wang, X., Hinnov, L.A., Qi, Y., Shen, S., Zhong Yang, T., Li, H., Chen, J., Zhang, S., 2019. An ~34 m.y. astronomical time scale for the uppermost Mississippian through Pennsylvanian of the Carboniferous System of the Paleo-Tethyan realm. Geology 47, 83–86. https://doi.org/10.1130/G45461.1.

Wu, H., Zhang, S., Jiang, G., Hinnov, L., Yang, T., Li, H., Wan, X., Wang, C., 2013b. Astrochronology of the Early Turonian-Early Campanian terrestrial succession in the Songliao Basin, northeastern China and its implication for long-period behavior of the Solar System. Palaeogeogr. Palaeoclimatol. Palaeoecol. 385, 55–70. https://doi.org/10.1016/j.palaeo.2012.09.004.

Yancheva, G., Nowaczyk, N.R., Mingram, J., Dulski, P., Schettler, G., Negendank, J.F.W., Liu, J., Sigman, D.M., Peterson, L.C., Haug, G.H., 2007. Influence of the intertropical convergence zone on the East Asian monsoon. Nature 445, 74–77. https://doi.org/10.1038/nature05431.

Yang, B., Steiner, M., Keupp, H., 2015. Early Cambrian palaeobiogeography of the Zhenba-Fangxian Block (South China): Independent terrane or part of the Yangtze Platform? Gondwana Res. 28, 1543–1565. https://doi.org/10.1016/j.gr.2014.09.020.

Yang, C., Li, X.H., Zhu, M., Condon, D.J., Chen, J., 2018. Geochronological constraint on the Cambrian Chengjiang Biota, South China. J. Geol. Soc. Lond. 175, 659–666. https://doi.org/10.1144/jgs2017-103.

Yeasmin, R., Chen, D., Fu, Y., Wang, J., Guo, Z., Guo, C., 2017. Climatic-oceanic forcing on the organic accumulation across the shelf during the early Cambrian (Age 2 through 3) in the mid-upper Yangtze Block, NE Guizhou, South China. J. Asian Earth Sci. 134, 365–386. https://doi.org/10.1016/j.jseaes.2016.08.019.

Zabel, M., Schneider, R.R., Wagner, T., Adegbie, A.T., De Vries, U., Kolonic, S., 2001. Late quaternary climate changes in Central Africa as inferred from terrigenous input to the Niger fan. Quat. Res. 56, 207–217. https://doi.org/10.1006/qres.2001.2261.

Zhai, L., Wu, C., Ye, Y., Zhang, S., Wang, Y., 2018. Fluctuations in chemical weathering on the Yangtze Block during the Ediacaran–Cambrian transition: Implications for paleoclimatic conditions and the marine carbon cycle. Palaeogeogr. Palaeoclimatol. Palaeoecol. 490, 280–292. https://doi.org/10.1016/j.palaeo.2017.11.006.

Zhang, S., Wang, X., Hammarlund, E.U., Wang, H., Costa, M.M., Bjerrum, C.J., Connelly, J.N., Zhang, B., Bian, L., Canfield, D.E., 2015. Orbital forcing of climate 1.4 billion years ago. Proc. Natl. Acad. Sci. U. S. A. 112, E1406–E1413. https://doi.org/10.1073/pnas.1502239112.

Zhang, R., Li, L., Nai, W., Gu, Y., Huang, C., Ogg, J., Li, Q., Lu, C., Wang, Z., 2019. Astronomical forcing of terrestrial climate recorded in the Pleistocene of the western Tarim Basin, NW China. Palaeogeogr. Palaeoclimatol. Palaeoecol. 530, 78–89. https://doi.org/10.1016/j.palaeo.2019.05.039.

Zhang, T., Li, Y., Fan, T., Da Silva, A.C., Shi, J., Gao, Q., Kuang, M., Liu, W., Gao, Z., Li, M., 2022. Orbitally-paced climate change in the early Cambrian and its implications for the history of the Solar System. Earth Planet. Sci. Lett. 583, 117420 https://doi.org/10.1016/j.epsl.2022.117420.

Zhao, Z., Thibault, N.R., Dahl, T.W., Schovsbo, N.H., Sørensen, A.L., Rasmussen, C.M.Ø., Nielsen, A.T., 2022. Synchronizing rock clocks in the late Cambrian. Nat. Commun. 13, 1–12. https://doi.org/10.1038/s41467-022-29651-4.

Zhong, Y., Wu, H., Zhang, Y., Zhang, S., Yang, T., Li, H., Cao, L., 2018. Astronomical calibration of the Middle Ordovician of the Yangtze Block, South China. Palaeogeogr. Palaeoclimatol. Palaeoecol. 505, 86–99. https://doi.org/10.1016/j.palaeo.2018.05.030.

Zhong, Y., Wu, H., Fan, J., Fang, Q., Shi, M., Zhang, S., Yang, T., Li, H., Cao, L., 2020. Late Ordovician obliquity-forced glacio-eustasy recorded in the Yangtze Block, South China. Palaeogeogr. Palaeoclimatol. Palaeoecol. 540, 109520 https://doi.org/10.1016/j.palaeo.2019.109520.

Zhu, M., Zhang, J., Steiner, M., Yang, A., Li, G., Erdtmann, B., 2003. Sinian-Cambrian stratigraphic framework for shallow- to deep-water environments of the Yangtze Platform: an integrated approach*. Prog. Nat. Sci. 13, 951–960. https://doi.org/10.1080/10020070312331344710.

Zhu, M., Zhang, J., Yang, A., 2007. Integrated Ediacaran (Sinian) chronostratigraphy of South China. Palaeogeogr. Palaeoclimatol. Palaeoecol. 254, 7–61. https://doi.org/10.1016/j.palaeo.2007.03.025.

Zhu, M., Yang, A., Yuan, J., Li, G., Zhang, J., Zhao, F., Ahn, S.Y., Miao, L., 2019. Cambrian integrative stratigraphy and timescale of China. Sci. China Earth Sci. 62, 25–60. https://doi.org/10.1007/s11430-017-9291-0.